



Original article



Nonlinear model predictive control for stabilizing tiltrotor urban air mobility aircraft under control effector failures

Jessica S.M. Nunes^a, Weihua Su^{a, ID, *}, Tianyi He^{b, ID}

^a Department of Aerospace Engineering and Mechanics, The University of Alabama, Tuscaloosa, AL, 35487-0280, United States

^b Department of Mechanical and Aerospace Engineering, Utah State University, Logan, UT, 84322-4130, United States

ARTICLE INFO

Communicated by Hever Moncayo

Keywords:

Nonlinear model predictive control
Tiltrotor aircraft
Urban air mobility
Fault-tolerant control
Flight safety

ABSTRACT

This paper demonstrates the effectiveness of a Nonlinear Model Predictive Controller (NMPC) for a tiltrotor urban air mobility aircraft experiencing failures of control effectors, specifically the elevator and tiltrotor, during its level flight. The vehicle's free-flight dynamic behavior is governed by a set of nonlinear rigid-body dynamic equations that account for multiple tiltrotors and their gyroscopic and inertial effects. The control variables include tiltrotors' spin and tilt kinematics and the traditional control surface deflections. Stability and performance of the NMPC are evaluated using the Monte Carlo approach, followed by a parametric study on rotor spin acceleration and tilt rate. From these studies, suitable rotor spin acceleration and tilt rate are determined for further control development with the elevator and asymmetric tiltrotor failure. The open-loop response is compared to NMPC and linear MPC for rudder failure, and NMPC for elevator failure. The results indicate that the NMPC can effectively attenuate the perturbation caused by an asymmetric tiltrotor failure by utilizing the back rotors as push thrusters. In contrast, linear MPC demonstrates limited performance with a narrow feasible region, making it less suitable for high-disturbance scenarios. When employing the back rotors for pitch control, the NMPC significantly reduces the phugoid mode vibrations caused by the elevator failure. Additionally, the findings suggest that when tilting the back rotors is necessary for pitch control, completing the tilting before spinning the rotors leads to improved path-tracking performance.

1. Introduction

The Urban Air Mobility (UAM) market is projected to experience significant growth driven by UAM's potential to revolutionize transportation of passengers, air ambulances, package delivery, law enforcement, and military operations [1]. These applications will have a considerable impact on services provided by both public and private institutions across various sectors. As the development progresses, enhancing flight safety, automation, and ride quality is more crucial than ever to integrate these new aircraft safely into urban airspace [2,3].

A key segment within UAM is the distributed electric propulsion (DEP) enabled vertical takeoff and landing (VTOL) vehicles, commonly known as eVTOLs. These vehicles employ a fixed-wing design with multiple tiltrotors to enable vertical takeoff and landing. The tilt and spin of

the rotors also function as actuators, enhancing safety through redundancy, i.e., with multiple rotors, these vehicles can continue operating even in case of motor or rotor failure, thereby reducing the risk of serious incidents.

Realizing these capabilities, however, depends on developing sophisticated control systems that can manage the unique complexities of eVTOL operations. For conventional aircraft, control in cases of surface failure often relies on pilot skill. While this is true, studies have been conducted on robust fault-tolerant control (FTC) systems capable of dealing with possible control surface failure [4,5]. Mabboux et al. [6] considered the motor failure of a UAV in a co-design process synthesizing the robust control law. However, such controls depend on rapidly identifying the nature of the failure, which is often difficult to do accurately during a flight. To address this, Wang et al. [7] proposed an adaptive fault-

* Corresponding author.

E-mail address: suw@eng.ua.edu (W. Su).

<https://doi.org/10.1016/j.ast.2025.110517>

Received 16 November 2024; Received in revised form 23 May 2025; Accepted 18 June 2025

Available online 26 June 2025

1270-9638/© 2025 Elsevier Masson SAS. All rights reserved, including those for text and data mining, AI training, and similar technologies.

Nomenclature

G	Global coordinate frame	I_B	Body moment of inertia..... kg·m ²
B	Body coordinate frame	m_r	Rotor mass..... kg
$\mathbf{p}_{G/B}$	Aircraft mass center in O_B m	I_r^e	Rotor moment of inertia..... kg·m ²
\mathbf{v}_B	Translational velocity vector..... m/s	β	Rigid-body velocity vector
ω_B	Angular velocity vector..... rad/s	ζ	Quaternions vector
θ_B	Rigid-body rotation angles..... rad	\mathbf{p}_B^G	Inertial position vector of O_B m
\mathbf{M}_{BB}	Inertia matrix	$\delta_e, \delta_a, \delta_r$	Elevator, aileron and rudder angles..... deg
\mathbf{C}_{BB}	Damping matrix	Ξ	Rotor tilt angle..... deg
\mathbf{R}_B	Aircraft load vector	Γ	Rotor spin angle..... deg
\mathbf{R}^{grav}	Gravity load	A, B, C	Continuous-time state space matrices
\mathbf{R}^{iner}	Inertial loads	A_d, B_d, C_d	Discrete-time state space matrices
\mathbf{R}^{rate}	Induced moment due to tiltrotors	dt	Discretization time step
\mathbf{R}^{gyro}	Gyroscopic loads	J	Cost function
\mathbf{R}^{ext}	External loads	p	Prediction horizon
Ω_ζ	Rigid-body angular velocities function	n	Control horizon
\mathbf{C}^{GB}	Rotational matrix - body to global	\mathbf{U}_k	Quadratic problem decision vector
\mathbf{x}	System states	\mathbf{r}	Output reference vector
\mathbf{u}	System control inputs	w^i	Variable i NMPC weight
\mathbf{y}	System outputs	s^i	Variable i NMPC scale factor
Φ	Euler angle vector	$u_{j,\text{target}}$	Target of the j^{th} input
ϕ	Roll angle..... deg	$\mathbf{u}_{\text{min/max}}$	Input limits vector
θ	Pitch angle..... deg	$\Delta\mathbf{u}_{\text{min/max}}$	Input rate limits vector
ψ	Yaw angle..... deg	\mathbf{Q}_M	Linear MPC state weight matrix
m_B	Body mass..... kg	\mathbf{R}_M	Linear MPC input weight matrix

tolerant control scheme with adaptive sliding-mode control to maintain tracking performance in both faulty and fault-free conditions. The adaptive scheme can automatically allocate control signals among abundant actuators. Another approach considered rotor failures as external disturbances, and a disturbance observer was designed to estimate rotor degradation. The estimated disturbance was then used in FTC to compensate for rotor degradation with guaranteed stability [8,9]. A more thorough review of the FTC of UAVs can be found in Ref. [10]. While several FTC techniques have been proposed for UAV applications, these methods often lack the ability to explicitly enforce state and actuator constraints, which is a critical requirement for eVTOL aircraft operating in complex urban environments.

Model Predictive Control (MPC) has the potential for eVTOL control, as it utilizes a model to predict future responses and determines optimal inputs for optimizing control objectives [11–13]. In the event of failure, MPC can successfully control aircraft or multi-rotor UAVs by explicitly incorporating constraints of states and actuators into the predictive models. Due to the nature of the nonlinear dynamics, Nonlinear Model Predictive Control (NMPC) has gained considerable attention. A fault-tolerant NMPC was designed in [14] to stabilize and control a quadrotor with a complete failure of a single rotor. The results demonstrated that NMPC could recover the damaged quadrotor even in the course of aggressive maneuvers. Similar fault-tolerant NMPCs were adopted in the works [15,16] for fixed-wing UAVs. To connect with estimation algorithms in practical implementations, nonlinear moving-horizon estimation or extended Kalman filter can be used to provide estimation of states and actuator faults [17,18]. These works study the rigid-body motions with a relatively simple dynamic model, focusing on amplifying the controller’s robustness against actuator failures. More recently, the authors investigated NMPC’s effectiveness for vibration suppression and lateral path tracking in a tiltrotor eVTOL [19]. In this study, NMPC performance was compared to open-loop (no controller), LQR, and linear MPC. Results showed that both NMPC and LQR effectively suppressed vibrations, whereas the linear MPC was ineffective in mitigating rigid-body oscillations. For path tracking, NMPC outperformed LQR, which relied on a linearized model of the tiltrotor dynamics, a limitation that contributed to its lower performance. In contrast, NMPC’s capacity to predict future

aircraft states and account for system nonlinearity enabled superior path tracking. However, the heavy computational burden associated with NMPC is worth mentioning, which usually limits its practical application.

Recently, Qu et al. [20] applied an adaptive MPC with Linear Parameter-Varying (LPV) models for the hovering control of a six-rotor eVTOL in scenarios involving motor failure. The nonlinear dynamic model of the VTOL aircraft was derived in [21], which will be used in this paper. The LPV models were developed by linearizing the nonlinear rigid-body model under varying failed rotor speeds. The LPV scheduling parameter was chosen as the failed rotor speed, considering the available motor peak power after failure to accurately represent the system’s state as it transitioned from a healthy to a failed condition. Results demonstrated that the adaptive MPC controller could recover and stabilize the aircraft after motor failure across all single-failure scenarios, outperforming linear MPC and highlighting the benefits of incorporating LPV into the controller design.

The dynamic behavior of aircraft is highly nonlinear when there is a failure in the control effector. Consequently, NMPC is a promising technique for analyzing failure and implementing fault-tolerant control in UAM aircraft. NMPC accounts for the fully nonlinear system, thereby eliminating the need for the linearization process required in MPC approaches that use linear or LPV models, which is often challenging to obtain linearized models about the transient nonlinear equilibrium states. Therefore, this paper seeks to expand this topic by studying the NMPC application for eVTOL aircraft control when the aircraft presents failure during flight. First, an analysis of the stability and performance of the NMPC is conducted using the Monte Carlo method, in which variations are applied to each system output to evaluate the controller’s ability to return the aircraft to its original trimmed flight condition. Next, the effects of rotor spin acceleration and tilt rate on flight control are examined, followed by the investigation of two failure scenarios: asymmetric tiltrotor failure and elevator failure during level flight.

This paper is organized as follows. Section 2 introduces the nonlinear flight dynamic formulation for tiltrotor aircraft, followed by the NMPC and linear MPC control systems description in Section 3. Section 4 shows the numerical results. Finally, conclusions are summarized in Section 5.

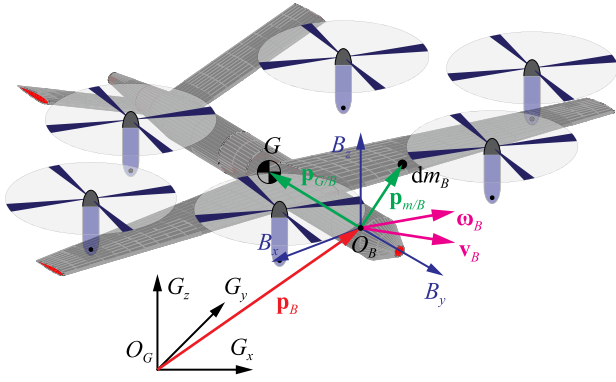


Fig. 1. Global and body reference frames of a rigid-body tiltrotor aircraft (connections between rotors and aircraft are not shown).

2. Flight dynamic formulations

This study investigates a hybrid urban air mobility (UAM) aircraft that consists of a fixed-wing airplane with tiltrotors (see Fig. 1). The study presents a condensed summary of these equations. One can refer to [21] for more details on the formulation.

A body-fixed frame B is defined with respect to the inertial frame G to describe the vehicle's position and orientation, with B_x pointing to the right wing, B_y pointing forward, and B_z completing the right-hand rule. While the B frame can be arbitrarily placed, it is convenient to set the frame's origin O_B within the vehicle's symmetric plane. The inertial position of O_B is represented by \mathbf{p}_B , while $\mathbf{p}_{G/B}$ describes the position of the mass center of the fixed-wing aircraft (excluding the tiltrotors) with respect to the B frame. The aircraft's rigid-body velocity is given by

$$\beta = \begin{Bmatrix} \mathbf{v}_B \\ \omega_B \end{Bmatrix} = \begin{Bmatrix} \dot{\mathbf{p}}_B + \omega_B \times \mathbf{p}_B \\ \theta_B \end{Bmatrix} \quad (1)$$

By following the Hamilton's principle, the governing equation of motion is obtained, given by

$$\mathbf{M}_{BB}(\Xi)\dot{\beta} + \mathbf{C}_{BB}(\beta, \Xi)\beta = \mathbf{R}_B \quad (2)$$

where the inertia matrix \mathbf{M}_{BB} is dependent on the tilt angles Ξ of the rotors, while the damping matrix \mathbf{C}_{BB} is dependent on both β and Ξ . The load vector \mathbf{R}_B is the summation of the loads about the B frame origin, including the contributions of gravity load $\mathbf{R}_B^{\text{grav}}$, inertial load $\mathbf{R}_B^{\text{iner}}$, induced moment due to tiltrotors $\mathbf{R}_B^{\text{rate}}$, gyroscopic load $\mathbf{R}_B^{\text{gyro}}$, and external load $\mathbf{R}_B^{\text{ext}}$, such as propulsive and aerodynamic loads, i.e.,

$$\mathbf{R}_B = \mathbf{R}_B^{\text{grav}} + \mathbf{R}_B^{\text{iner}} + \mathbf{R}_B^{\text{rate}} + \mathbf{R}_B^{\text{gyro}} + \mathbf{R}_B^{\text{ext}} \quad (3)$$

where details of the loads can be found in [21]. In addition, the B frame's orientation is described by the quaternions ζ , governed by

$$\dot{\zeta} = -\frac{1}{2}\Omega_\zeta(\beta)\zeta \quad (4)$$

where Ω_ζ is a function of the rigid-body angular velocities ω_B . Lastly, the inertial position of the B frame can be calculated by

$$\dot{\mathbf{p}}_B^G = \mathbf{C}^{GB}\mathbf{v}_B = [\mathbf{C}^{GB} \quad \mathbf{0}_3] \beta \quad (5)$$

where \mathbf{C}^{GB} is the rotational transformation matrix from the body to the global frame. The combination of Eqs. (2), (4), and (5) completes the nonlinear flight dynamic model of the tiltrotor UAM aircraft. Those equations can be transformed to

$$\begin{aligned} \dot{\beta} &= \mathbf{M}_{BB}^{-1}(-\mathbf{C}_{BB}(\beta, \Xi)\beta + \mathbf{R}_B(\beta, \zeta, \delta_e, \delta_a, \delta_r, \Xi, \Gamma)) \\ \dot{\zeta} &= -\frac{1}{2}\Omega_\zeta(\beta)\zeta \\ \dot{\mathbf{p}}_B^G &= [\mathbf{C}^{GB} \quad \mathbf{0}_3] \beta \end{aligned} \quad (6)$$

where δ_e , δ_a and δ_r are the elevator, aileron, and rudder deflections, Ξ is the vector containing the rotor's tilt angles, and Γ is the vector of spin kinematics of the rotors. Therefore, the nonlinear system state and control input vectors are defined as follows,

$$\begin{aligned} \mathbf{x}^T &= \left\{ \beta^T \quad \zeta^T \quad (\mathbf{p}_B^G)^T \right\} \\ \mathbf{u}^T &= \left\{ \delta_e \quad \delta_a \quad \delta_r \quad \Xi^T \quad \dot{\Xi}^T \quad \ddot{\Xi}^T \quad \dot{\Gamma}^T \quad \ddot{\Gamma}^T \right\} \end{aligned} \quad (7)$$

As a post-processing, the Euler angles can be calculated from the quaternions. By keeping the convention of the Euler angles defined in the north-east-down (NED) frame for flight dynamics, the yaw angle ψ is defined as rotation about negative B_z -axis, the pitch angle θ is defined as rotation about B_x -axis, and the roll angle φ is defined as rotation about B_y -axis. Therefore, the Euler angles are given by

$$\begin{aligned} \varphi &= \tan^{-1} \frac{2(\zeta_1\zeta_2 - \zeta_0\zeta_3)}{1 - 2(\zeta_0^2 + \zeta_1^2)} \\ \theta &= \sin^{-1} [-2(\zeta_1\zeta_3 + \zeta_0\zeta_2)] \\ \psi &= \tan^{-1} \frac{2(\zeta_0\zeta_1 - \zeta_2\zeta_3)}{1 - 2(\zeta_1^2 + \zeta_2^2)} \end{aligned} \quad (8)$$

which can be simply noted as

$$\Phi = \{\varphi \quad \theta \quad \psi\}^T = \Phi(\zeta). \quad (9)$$

Additionally, the system output \mathbf{y} can be selected as a combination of system states and Euler angles, with the full form given by

$$\mathbf{y}^T = \left\{ \beta^T \quad \Phi^T \quad (\mathbf{p}_B^G)^T \right\} \quad (10)$$

The trim solutions, either for level flight or vertical takeoff, were introduced in Ref. [21], which provide the steady-state solutions of the nonlinear equation set presented. In general, one can take the Taylor's expansion on the nonlinear governing equations with respect to a nonlinear equilibrium \mathbf{e}_0 with control input u_0 . The linearized equation, as well as the procedure to discretize the state-space system, are presented in [19]. Therefore, this will be omitted here. The result is the discrete system below with the Δ omitted

$$\begin{aligned} \mathbf{x}_{k+1} &= \mathbf{A}_d \mathbf{x}_k + \mathbf{B}_d \mathbf{u}_k \\ \mathbf{y}_{k+1} &= \mathbf{C} \mathbf{x}_k \end{aligned} \quad (11)$$

3. Control development

3.1. Nonlinear model predictive controller

The nonlinear model predictive controller (NMPC) looks ahead by p steps to predict the system responses in the future (predicted output in Fig. 2). It calculates the best sequence of control inputs \mathbf{u} from the present to $t_n = t + n \times dt$ to achieve the closest match between the system output and the desired output reference (predicted control input in Fig. 2) [22]. Here, p is the prediction horizon, and n is the control horizon illustrated in Fig. 2. At each time step, the controller predicts the future system output and solves an optimization problem to determine the control input, using only the initial input vector (orange line). This procedure is repeated in the next time step. This approach significantly enhances controller performance with the trade-off of increased computational cost.

In this study, the NMPC is designed using the MATLAB[®] function *nlmpc*, where the function *nlmpcmove* solves the quadratic problem and find the optimal control input in each time step. The cost function of the quadratic problem is

$$J(\mathbf{U}_k) = J_y(\mathbf{U}_k) + J_u(\mathbf{U}_k) + J_{\Delta u}(\mathbf{U}_k) \quad (12)$$

where \mathbf{U}_k is the quadratic problem decision defined by

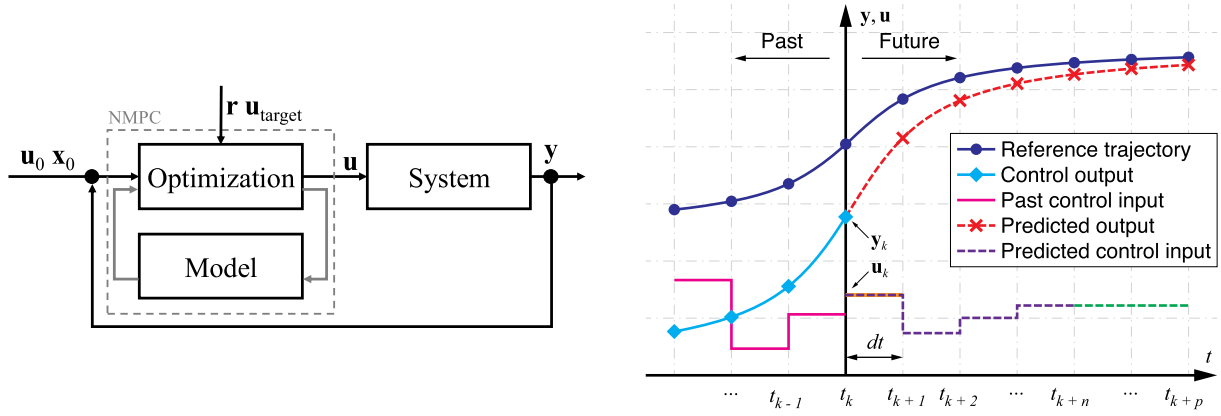


Fig. 2. Simplified NMPC block diagram and example of controller with control and prediction horizons. (For interpretation of the colors in the figure(s), the reader is referred to the web version of this article.)

$$\mathbf{U}_k^T = \{ \mathbf{u}^T(k|k) \quad \mathbf{u}^T(k+1|k) \quad \dots \quad \mathbf{u}^T(k+p-1|k) \} \quad (13)$$

The \mathbf{U}_k^T vector contains the inputs vectors $\mathbf{u}^T(k+i-1|k)$ calculated in the current control interval k for the i^{th} prediction horizon step, where i ranges from 1 to the prediction horizon p defined during the controller design. The output reference tracking term J_y given by

$$J_y(\mathbf{U}_k) = \sum_{j=1}^{n_y} \sum_{i=1}^p \left\{ \frac{w_{i,j}^y}{s_j^y} [r_j(k+i|k) - y_j(k+i|k)] \right\}^2 \quad (14)$$

relates the j^{th} output reference $r_j(k+i|k)$ to the j^{th} output $y_j(k+i|k)$, both referent to the i^{th} prediction horizon calculated at the current control interval k . The minimization of this term can be tuned by adjusting the weight for j^{th} plant output at the i^{th} prediction horizon step $w_{i,j}^y$ and the scale factor of the j^{th} output s_j^y . The cost function term J_u allows for the input variable tracking and is given by

$$J_u(\mathbf{U}_k) = \sum_{j=1}^{n_u} \sum_{i=0}^{p-1} \left\{ \frac{w_{i,j}^u}{s_j^u} [u_j(k+i|k) - u_{j,target}(k+i|k)] \right\}^2 \quad (15)$$

where $u_{j,target}$ is the target value for the j^{th} input. $w_{i,j}^u$ and s_j^u are the weight and the scale factor of the j^{th} input. The third term of the cost function is

$$J_{\Delta u}(\mathbf{U}_k) = \sum_{j=1}^{n_u} \sum_{i=0}^{p-1} \left\{ \frac{w_{i,j}^{\Delta u}}{s_j^{\Delta u}} [u_j(k+i|k) - u_j(k+i-1|k)] \right\}^2 \quad (16)$$

which allows for the consideration of input move smoothness during the optimization process.

The NMPC is tuned for each case studied by adjusting the output and input weights. Those are considered constant throughout the prediction and control horizons and therefore have the new form w_j^y and w_j^u for the j^{th} output and j^{th} input weights. All the scale factors mentioned are kept at their default value of 1. The input movement weights $w_{i,j}^{\Delta u}$ are also kept at their default values of 0.1. While the NMPC formulation allows for output constraints, only input and input rate hard constraints are used in this work, i.e.,

$$u_{j,\min}(i) \leq u_j(k+i-1|k) \leq u_{j,\max}(i) \quad (17)$$

$$\Delta u_{j,\min}(i) \leq \Delta u_j(k+i-1|k) \leq \Delta u_{j,\max}(i)$$

The scale factors were omitted from Eq. (17) since they were kept as units. In addition, uncertainties, and measured and unmeasured disturbances are neglected in the current work. In other words, the sensor data is assumed to be perfect reading without the noise on sensor read-

ings. The effectiveness of the NMPC controller with uncertainties will be studied in future work.

3.1.1. NMPC tuning

The NMPC is tuned by adjusting the output and input weights w_j^y and w_j^u . Increasing the output weights for a specific output enhances reference tracking for that output. In contrast, higher input weights impose a greater penalty on input variations, keeping them closer to the input target values. Although this stabilizes the system and keeps inputs within desirable ranges, it may also limit adaptability to unforeseen disturbances. Achieving a balance between precise output tracking and input flexibility is essential for enhancing overall system performance. Weights were tuned on a trial-and-error basis and experience from previous studies.

Additionally, the definition of input constraints is essential for the proper behavior of the NMPC. Implementing these constraints can significantly reduce computational costs and enhance control accuracy. Without input constraints, system inputs tend to exceed the saturation threshold of actuators, which can pose risks during operation. Conversely, over-constrained systems can lead to an unsolvable optimization problem without a feasible control solution. When it becomes impossible to satisfy all constraints simultaneously, the NMPC prioritizes one constraint over others. However, this prioritization can change abruptly, resulting in a potential loss of control. Therefore, carefully considering input constraints is crucial for ensuring stable and reliable system performance. Section 4.2 and Section 4.3 present a study of the constraint boundaries for rotor spin acceleration and tilt velocity, respectively. For each case examined, the NMPC input limits are adjusted accordingly. The configuration that demonstrates the best performance while preserving realistic constraint boundaries is adopted in the subsequent sections.

The prediction and control horizons play a crucial role in the effectiveness of NMPC. A larger prediction horizon allows the controller to anticipate future system behavior more accurately, improving overall performance. Although a control horizon of one is typically selected for most applications without significantly affecting results, increasing the prediction horizon can enhance long-term responses. However, this comes at the cost of a substantial increase in computational demand.

Alternatively, increasing the simulation time step can extend the prediction range into the future, but at the risk of reduced numerical accuracy. This can lead to the loss of critical dynamic behavior and potentially result in instability or divergence in the simulation.

In this work, a prediction horizon of 10, a control horizon of 1, and a time step of 0.1 s are used. While this configuration yields good performance (Sec. 4), the high computational cost remains a significant challenge (see Sec. 4.6). Therefore, a comprehensive study on controller

computation optimization, including a parametric analysis of the time step, control horizon, and prediction horizon, is necessary.

3.2. Linear model predictive controller

The linear Model Predictive Controller (MPC) operates in a similar way to the NMPC. It predicts future system responses over a prediction horizon p and computes an optimal sequence of control inputs over a control horizon n to closely track the desired output reference (see Fig. 2). However, unlike NMPC, linear MPC uses the linear system in its discrete-time form presented in Eq. (11). Therefore, the cost function to be minimized for the linear MPC is given by

$$J(\mathbf{U}_k) = \mathbf{y}_n^T \mathbf{Q}_f \mathbf{y}_n + \sum_{k=0}^{n-1} (\mathbf{y}_k^T \mathbf{Q}_M \mathbf{y}_k + \mathbf{u}_k^T \mathbf{R}_M \mathbf{u}_k) \quad (18)$$

where \mathbf{Q}_f is the terminal weighting matrix assumed to be an identity matrix, and \mathbf{Q}_M and \mathbf{R}_M are the states and control input weight matrices for the MPC [23]. The weight matrices are assumed to be diagonal matrices. \mathbf{U}_k represents the control input sequence up to the control horizon, which is to be obtained from the problem minimization (see Eq. (13)).

In addition, the inputs are also subject to the hard constraints

$$\begin{aligned} \mathbf{u}_{min} &\leq \mathbf{u}(t_k) \leq \mathbf{u}_{max} \\ \Delta \mathbf{u}_{min} &\leq \mathbf{u}(t_{k+1}) - \mathbf{u}(t_k) \leq \Delta \mathbf{u}_{max} \end{aligned} \quad (19)$$

where $\mathbf{u}(k)$ is the control input vector at time t_k . An infeasible problem can occur when the controller cannot satisfy the optimization problem constraints. This means that it is mathematically impossible to meet the hard constraints while following the steady-state system equation (Eq. (11)). Infeasibility may be due to an over-constrained system or a significant system disturbance, which can render the MPC unable to effectively control the dynamic system.

3.2.1. Linear MPC tuning

The linear MPC prediction horizon and time step are chosen to match those of the NMPC, 10 and 0.1 s respectively, to enable a fair, apples-to-apples comparison between the two controllers. Similarly, the input limits are kept consistent with those used in the NMPC formulation.

The \mathbf{Q}_M and \mathbf{R}_M matrices are tuned similarly to the tuning process of the input and output weights of the NMPC. The \mathbf{Q}_M matrix is a diagonal matrix with the state weights, where larger values in $Q_{M,i}$ indicate a higher penalty for deviations of that state from the desired trajectory. \mathbf{R}_M is also assumed to be a diagonal matrix, with each diagonal element representing the weight assigned to a particular control input. Larger values in $R_{M,i}$ indicate a higher penalty for control effort.

4. Numerical studies

This study focuses on the control of a fixed-wing UAM aircraft with six tiltrotors, as shown in Fig. 3. The aircraft's inertial and aerodynamic properties are listed in Tables 1 and 2, respectively. The rigid propeller pylon length is assumed to be 1 m. A comprehensive trim analysis at multiple flight conditions and the validation of the rotor tilt transition flight were investigated in a previous study (Ref. [21]) and will not be discussed here. The results showed that the aircraft model studied is stable and that the formulation can capture the essential characteristics of rotor kinematics, such as tilt angle and spin rate, regarding the overall vehicle response.

Moreover, previous research [19] investigated the comparison of NMPC with both LQR and linear MPC. That study analyzed the performance of all three controllers in mitigating rigid-body phugoid mode oscillations following elevator input excitation. While all three controllers reduced oscillations compared to the open-loop response, MPC was ineffective in fully attenuating the rigid-body oscillation, failing

to eliminate it over an 80 s simulation. Even when excitation magnitudes were reduced by 30%, MPC remained unsuccessful in completely suppressing the oscillations, demonstrating its unsuitability for eVTOL applications exhibiting highly nonlinear dynamics. Subsequently, LQR and NMPC were compared in lateral and longitudinal path-tracking scenarios. Unlike the previous case, LQR could no longer maintain the desired trajectory. In contrast, NMPC, leveraging its predictive capabilities and ability to account for system nonlinearities, achieved superior path-tracking performance. Based on these findings, this study further assesses the viability of NMPC for eVTOL applications by investigating its effectiveness in maintaining level flight when subjected to effector failure.

The study includes an analysis of the NMPC stability and performance through the Monte Carlo method in Sec. 4.1. This study aims to assess the NMPC stability and performance when subjected to state disturbances. The impact of tiltrotor spin acceleration on NMPC flight control in Sec. 4.2, and an evaluation of NMPC for different rotor tilt rates in Sec. 4.3 is also conducted. Based on the findings from these studies, the effectiveness of NMPC is examined in two failure cases, each considering rotor tilt and no tilt needed:

- Asymmetric tiltrotor failure during level flight (Sec. 4.4)
- Elevator failure during level flight (Sec. 4.5)

The NMPC is compared to the MPC for the case of asymmetric tiltrotor failure without rotor tilting in Sec. 4.4.1.

These cases were selected to reflect distinct but critical failures that can significantly impact eVTOL flight stability and control performance. The asymmetric tiltrotor failure simulates a loss of thrust or effectiveness in one of the rotors, leading to asymmetric aerodynamic forces and control challenges, particularly in yaw and roll. This scenario is especially relevant for distributed electric propulsion systems, where the failure of a single rotor can cause considerable disturbances despite system redundancy.

The elevator failure represents a typical control surface fault that can significantly compromise pitch stability and longitudinal trim, particularly during cruise flight. Although eVTOLs primarily rely on rotor-based control in hover, aerodynamic control surfaces such as the elevator play a critical role during forward flight phases. While not all potential failure modes are explored in this study, the selected cases, which cover both rotor-based (propulsion) and aerodynamic control failures, capture key challenges relevant to eVTOL operations. These representative scenarios provide a strong foundation to demonstrate the NMPC's effectiveness and its potential for fault-tolerant control across a broad range of practical conditions.

It is important to note that the current framework assumes prior fault knowledge. Faults are not detected in real time, and the controller is updated based on this assumption. Specifically, output weights remain constant after a fault, while input weights are adjusted to reflect the presence of failed actuators and to improve control performance (see Appendix). This allows the controller to reallocate effort among the remaining actuators and maintain acceptable trajectory tracking. Although this method clearly demonstrates the NMPC's capabilities, it does not yet reflect a fully autonomous system. A real-time fault detection algorithm should be integrated into the control loop for future implementations to enable adaptive responses to unforeseen failures.

To address differences in input scaling and improve convergence behavior, the NMPC formulation uses the input increment $\Delta \mathbf{u}(k)$ as controller input, defined as

$$\begin{aligned} \Delta \mathbf{u}(k) &= \mathbf{u}(k) - \mathbf{u}(k-1) \\ \Delta \mathbf{u}_{target}(k+1) &= \mathbf{u}_{target}(k) - \mathbf{u}(k) \end{aligned} \quad (20)$$

Here, $\mathbf{u}(k)$ is the current input vector, and $\mathbf{u}_{target}(k)$ is the desired steady-state input. This desired input is computed through solving the differential equation of Eq. (6), assuming a given flight speed and alti-

Table 1
Inertial properties of UAM aircraft.

Inertial Property	Value	Unit
Body mass, m_B	2,240.73	kg
Body moment of inertia, $I_{B,xx}$	12,000	kg m ²
Body moment of inertia, $I_{B,yy}$	9,400	kg m ²
Body moment of inertia, $I_{B,zz}$	20,000	kg m ²
Rotor mass, m_r	4.55	kg
Rotor moment of inertia, $I_{r,xx}^e$	3.5	kg m ²
Rotor moment of inertia, $I_{r,yy}^e$	7.0	kg m ²
Rotor moment of inertia, $I_{r,zz}^e$	3.5	kg m ²

Table 2
Aerodynamic properties of UAM aircraft.

Aerodynamic Property	Wing	Tail
Airfoil	NACA 0012	NACA 0012
Ref. axis location *	25%	25%
Span [m]	13.72	6.90
Sweep angle [°]	-2.306	0
Dihedral angle [°]	0	0
Chord (root/tip) [m]	2.075/0.970	1.080/1.080
Incidence angle [°]**	3.1598	1.0626

* From leading-edge
** Incident angle with no twist

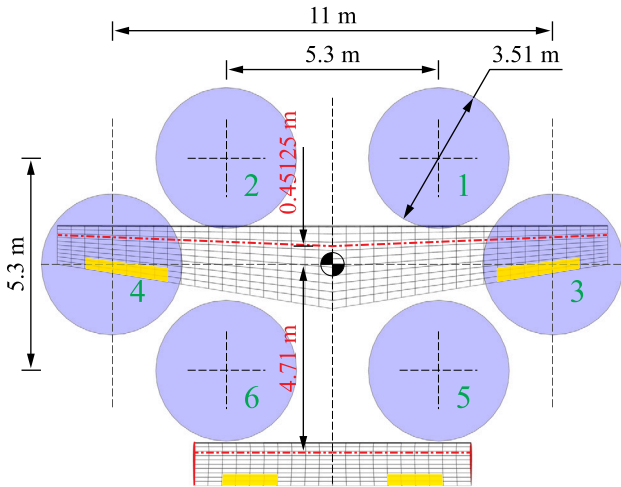


Fig. 3. Tiltrotor UAM aircraft geometry and rotor positions.

tude (68 m/s and 304.8 m). Rotors on/off as well as tilt position are also predefined. Additionally, to assure steady-state flight, aileron and rudder inputs, as well as all inputs 1st and 2nd order derivatives, are equal to zero. With those constraints, solving the equation becomes trivial, solving for spin rates and elevator input only, which then become the $\mathbf{u}_{\text{target}}(k)$.

By minimizing the cost function term based on the difference $\Delta \mathbf{u} - \Delta \mathbf{u}_{\text{target}}$, the controller not only moves the input toward its target but also encourages convergence to a steady-state condition (i.e., $\mathbf{u}(k) = \mathbf{u}(k-1)$). When the input reaches its target, $\Delta \mathbf{u}_{\text{target}}$ becomes zero, and the control action naturally stabilizes.

Since $\Delta \mathbf{u}$ represents relative changes rather than absolute magnitudes, inputs with vastly different numerical scales (e.g., elevator deflections vs. rotor speeds) do not disproportionately affect the cost function. Moreover, penalizing input increments helps reduce unnecessary oscillations and promotes convergence to the desired input state. This design facilitates smoother and more balanced control actions across different

actuators, especially in systems with heterogeneous inputs, such as eVTOL aircraft.

The NMPC states \mathbf{x} and output \mathbf{y} are kept at full parameter values. For all the cases, they are given by

$$\mathbf{x}^T = \left\{ \beta^T \quad \zeta^T \quad (\mathbf{p}_B^G)^T \right\} \quad (21)$$

$$\mathbf{y}^T = \left\{ \phi \quad \theta \quad \psi \quad p_{B,x}^G \quad p_{B,z}^G \right\}$$

where ϕ , θ , and ψ are the roll, pitch, and yaw angles in degrees. $p_{B,x}^G$ is the B 's frame inertial position in the lateral (East) direction measured in meters, while $p_{B,z}^G$ is the altitude.

The controllers' inputs and configuration settings for each case are summarized in the Appendix. The control input vector \mathbf{u} may include elevator, aileron, rudder, the spin rates of rotors 3 through 6, and the tilt angles of rotors 5 and 6, as illustrated in Fig. 3. Rotors 3 and 6 rotate in the counterclockwise direction (negative spin rates), while rotors 4 and 5 rotate clockwise (positive spin rates). A tilt angle Ξ_i of 0° corresponds to a forward-facing rotor, while 90° indicates an upward-facing rotor, consistent across all rotors.

The NMPC is simulated using a time step of 0.1 s, and *fmincon* as the optimization problem solver from MATLAB's Optimization Toolbox. A case ID will be used for simulation identification. It follows the naming convention 1-2-3-3-4 where 1 means open-loop (O), MPC (M), or NMPC (N) simulations. The information on failure type is given on 2, with FE for elevator failure and FR for rotor. 2 can also be used to specify Monte Carlo study results (MC). 3 provides additional information on the case, such as the spin acceleration or others. Lastly, 4 informs on the initial position of the back rotors when applicable (rotors 5 and 6 in Fig. 3), with F meaning forward and U upward.

For all cases, the aircraft is initially brought to a trimmed level flight with the speed of 68 m/s at the altitude of 304.8 m. Rotors 3 and 4 operate as the push rotors to provide the thrust. Rotors 1 and 2 are never used, while rotors 5 and 6 can be engaged if a push rotor malfunction occurs. The NMPC input target after failure is determined by solving the differential equation of Eq. (6) with said failure, resulting in the input vector needed for a trimmed flight in this configuration. This information is provided to the NMPC, which is tasked with stabilizing the flight in the event of a failure with a minimum deviation from the initial flight

Table 3
Monte Carlo data summary.

Property	Variation	Unit	t_{conv} (s) [*]	Input	Note
Eastward velocity, $v_{B,x}$	± 5	m/second	5.2	δ_r, δ_a	Converged
Northward velocity, $v_{B,y}$	$\pm 5\% \times v_{B,y,0}$	m/s	5.8	δ_e	Converged to diff. value
Vertical velocity, $v_{B,z}$	± 5	m/s	5.7	δ_e	Converged
X angular velocity, $\omega_{B,x}$	± 5	$^\circ/s$	5.4	δ_e	Converged
Y angular velocity, $\omega_{B,y}$	± 5	$^\circ/s$	3.3	δ_a, δ_r	Converged
Z angular velocity, $\omega_{B,z}$	± 2	$^\circ/s$	6.9	$\delta_r, \delta_a, \delta_e$	Converged, solution not found for var. $> 2^\circ$
Roll angle, ϕ	± 5	$^\circ$	4.3	$\delta_r, \delta_a, \delta_e$	Converged
Pitch angle, θ	± 5	$^\circ$	5.2	δ_e	Converged
Yaw angle, ψ	± 5	$^\circ$	6.5	δ_r	Converged
Eastward position, $p_{B,x}^G$	± 5	m	-	δ_r	Not fully converged
Northward position, $p_{B,y}^G$	± 5	m	2.3	δ_e	Converged
Vertical position, $p_{B,z}^G$	± 5	m	5.2	δ_e	Converged

^{*} Time taken to converge

path. That desired path is a straight and level flight in the y (North) direction.

When tiltrotors are used to stabilize the aircraft flight, their transient kinematics, including the rotor spin acceleration and tilt rate, may impact the behavior of the controlled flight. In Sec. 4.2 and 4.3, parametric studies are carried out to determine feasible transient rotor kinematics.

4.1. Study on controller stability

The Monte Carlo method for determining controller stability is a probabilistic approach used to evaluate how likely it is that a control system remains stable under uncertainty. Monte Carlo methods simulate a large number of system instances with random variations in parameters within a realistic range, and then check stability for each instance.

The system inputs, outputs, and states used in this study are given by

$$\begin{aligned} \mathbf{x}^T &= \left\{ \beta^T \quad \zeta^T \quad (\mathbf{p}_B^G)^T \right\} \\ \mathbf{y}^T &= \left\{ \beta^T \quad \Phi^T \quad (\mathbf{p}_B^G)^T \right\} \\ \mathbf{u}^T &= \Delta \left\{ \delta_e \quad \delta_a \quad \delta_r \quad \Xi_5 \quad \Xi_6 \quad \dot{\Gamma}_3 \quad \dot{\Gamma}_4 \quad \dot{\Gamma}_5 \quad \dot{\Gamma}_6 \right\} \end{aligned} \quad (22)$$

All simulations are initialized using the conditions described in Sec. 4, corresponding to trimmed level flight at a speed of 68 m/s and an altitude of 304.8 m, heading due north. Rotors 3 and 4 serve as the push rotors, providing the primary thrust. Rotors 1 and 2 are turned off for the entire simulation duration. Rotors 5 and 6 are initially off and oriented forward, but their spin velocity and tilt angles are available control inputs throughout the simulation.

This study investigates the system's response to variations in each output \mathbf{y} . Ideally, all 12 outputs would be subjected to random variations across their feasible ranges. However, to reduce the number of required simulations, a more constrained yet representative range of output variations was selected, as detailed in Table 3. The chosen ranges are designed to be sufficiently large to present a challenge for the eV-TOL system, while still reflecting variations that are plausible under real operational conditions.

The simulation are initially in trimmed flight condition, and at 0.5 s, the output variations are included and the controller is tasked with returning the aircraft to the trimmed flight condition. The NMPC output weight, which determines the priority given to tracking a specific output, is selected to be 0.8 for all outputs and 5 for the output with variation applied. The input weights are uniformly set to 0.2 for all control inputs. Each output variation is introduced individually, and the results for the worst cases, typically occurring at the extremes of the variation range, are presented in Table 3.

The results show that the controller is stable and able to converge to the desired values for most outputs, with a fast response time of less than

7 s. However, a few exceptions are observed. For the northward velocity $v_{B,y}$, which corresponds to the flight direction, the NMPC remains stable and reaches a steady value after approximately 5.8 s. However, in the worst-case scenario, the final value deviates by 0.95 m/s from the desired velocity of 68 m/s. For the angular velocity $\omega_{B,z}$, the NMPC is able to achieve convergence only for variations within $\pm 2^\circ$. For variations beyond this threshold, the system becomes infeasible, and the controller is unable to maintain stability. Lastly, the eastward position $p_{B,x}^G$, which represents the aircraft position due East, also posed a challenge. Although the controller exhibits a clear trend toward convergence, it is unable to fully stabilize the output to a constant value by the end of the 30 s simulation. In no case is divergence observed.

To further evaluate the controller's stability, more demanding scenarios are considered, involving simultaneous disturbance of multiple outputs in both longitudinal and lateral directions. The corresponding case IDs and descriptions are provided in Table 4. The specific NMPC settings used for these multi-variable cases are summarized in the Appendix.

4.1.1. Monte Carlo approach: longitudinal disturbance

The following output variations are applied at 0.5 ms of simulation

- Pitch angle, θ : $+5^\circ$
- Vertical velocity, $v_{B,z}$: $+5$ m/s
- Vertical position, $p_{B,z}^G$: $+5$ m

and the controller is tasked with returning the aircraft to the trimmed flight condition.

The results shown in Fig. 5 indicate that the NMPC primarily relies on elevator deflection to correct deviations in altitude, vertical velocity, and pitch angle. Fig. 4 shows that all variables are successfully driven back to stable values near the initial conditions within approximately 10 s. In contrast, the open-loop results illustrate that, without control intervention, the system would exhibit sustained oscillations in both altitude and pitch angle.

4.1.2. Monte Carlo approach: lateral disturbance

For this case, the outputs related to lateral motion, listed below, are disturbed at 0.5 s into the simulation.

- Yaw angle, ψ : $+5^\circ$
- Roll angle, ϕ : $+5^\circ$
- Eastward velocity, $v_{B,x}$: $+5$ m/s
- Eastward position, $p_{B,x}^G$: $+5$ m

This scenario presents a significant challenge, as it involves the simultaneous excitation of multiple variables, including the eastward position, output with worse results when disturbed individually. Nev-

Table 4
Case ID and descriptions for Monte Carlo study.

Case ID	Description
O-MC-LON	Open loop results for Monte Carlo analysis under longitudinal disturbances
O-MC-LAT	Open loop results for Monte Carlo analysis under lateral disturbances
N-MC-LON	NMPC results for Monte Carlo analysis under longitudinal disturbances
N-MC-LAT	NMPC results for Monte Carlo analysis under lateral disturbances

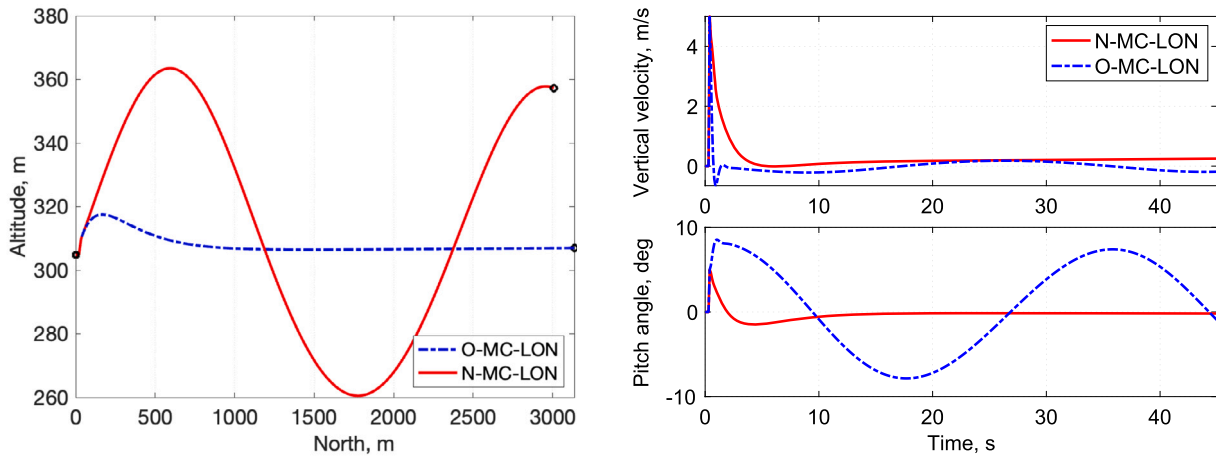


Fig. 4. Aircraft trajectory and Euler angle response during flight subjected to longitudinal disturbance.

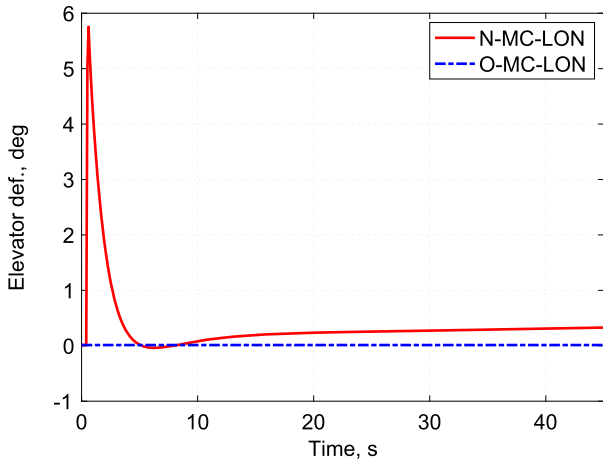


Fig. 5. Control surface inputs during flight subjected to longitudinal disturbance.

ertheless, the results shown in Figs. 6 to 8 demonstrate a substantial improvement over the open-loop response. The Euler angles successfully converge to their initial conditions, and while the eastward position still exhibits a maximum deviation of 9.6 m, it represents a marked improvement compared to the uncontrolled case. Notably, the lateral excitation induces secondary deviations in altitude and pitch angle, as the controller prioritizes correcting higher-weighted variables (ψ , ϕ , $v_{B,x}$, and $p_{B,x}^G$).

Overall, the controller exhibits robust performance, with very few instances of divergence or instability. These results support its reliability in managing nominal flight conditions, justifying this study's focus on assessing this controller's performance with fault tolerance.

4.2. Tiltrotor spin acceleration study

This study explores how the rotor spin acceleration impacts the stabilization of a vehicle with a push rotor failure. Refer to Fig. 3. After

Table 5

Case ID and descriptions for rotor spin acceleration parametric study.

Case ID	Description
O-FR-F	Open loop
N-FR-S300-F	NMPC - Rotor spin acceleration of 300 deg/s ²
N-FR-S500-F	NMPC - Rotor spin acceleration of 500 deg/s ²
N-FR-S1000-F	NMPC - Rotor spin acceleration of 1000 deg/s ²
N-FR-S2000-F	NMPC - Rotor spin acceleration of 2000 deg/s ²
N-FR-S3000-F	NMPC - Rotor spin acceleration of 3000 deg/s ²

a failure in rotor 3 is detected, rotors 5 and 6 are used to stabilize the vehicle. Before the failure occurs, push rotors 3 to 6 are facing forward ($\Xi_{3:6} = 0^\circ$) with only rotors 3 and 4 active. At $t = 3$ s, rotor 3 fails (i.e., spin rate changes to zero) as shown in Fig. 9, while rotor 4 is still operating. It causes the aircraft to yaw due East and lose altitude rapidly, as shown in Fig. 10. The black cross on the curve indicates the moment when the aircraft crashes.

At the instant of failure ($t = 3$ s), rotors 5 and 6 become the control input for NMPC to stabilize the vehicle. Five spin accelerations are compared, including 300, 500, 1000, 2000, and 3000 deg/s². The case IDs and descriptions are listed in Table 5 and the corresponding NMPC settings are presented in the Appendix. Nonetheless, the NMPC input vector is

$$\mathbf{u}^T = \Delta \{ \delta_e \quad \delta_a \quad \delta_r \quad \dot{\Gamma}_3 \quad \dot{\Gamma}_4 \quad \dot{\Gamma}_5 \quad \dot{\Gamma}_6 \} \quad (23)$$

where $\dot{\Gamma}_i$ are the spin rates of rotors 3 to 6.

Figs. 11 and 12 illustrates the control inputs of each simulated case listed in Table 5, which includes the spin rate of rotors 4 to 6, elevator, aileron, and rudder deflection angles. In the open-loop scenario, the inputs remain constant throughout the simulation. In contrast, in the controlled cases, rotor 4 is turned off as quickly as possible, subject to the defined spin acceleration limit. The shutdown of rotor 4 can prevent the aircraft from yawing eastward, a behavior observed in the open-loop response. Meanwhile, rotors 5 and 6 spin up to provide the thrust. While symmetric control forces are achieved eventually, the aircraft still devi-

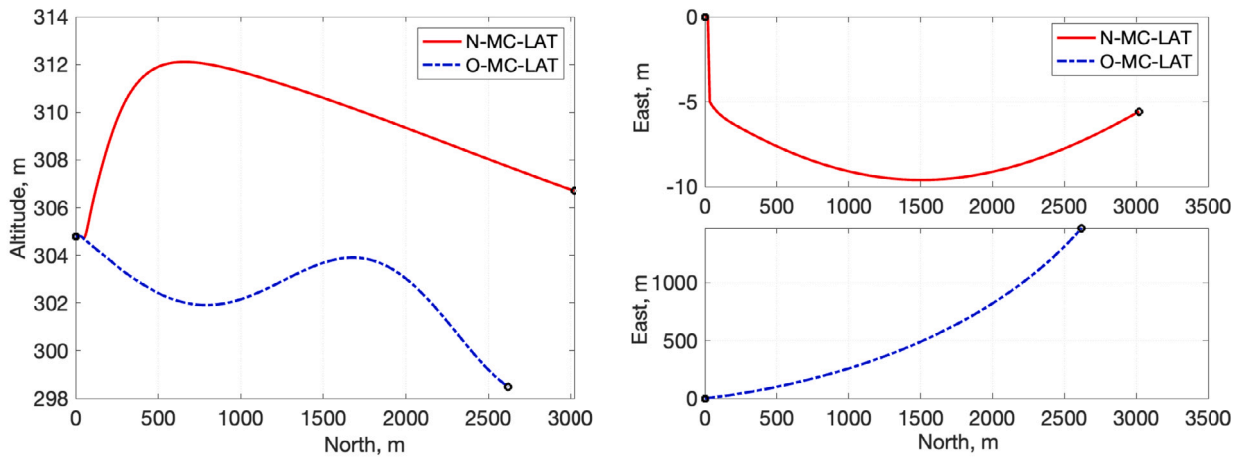


Fig. 6. Aircraft trajectory response during flight subjected to lateral disturbance.

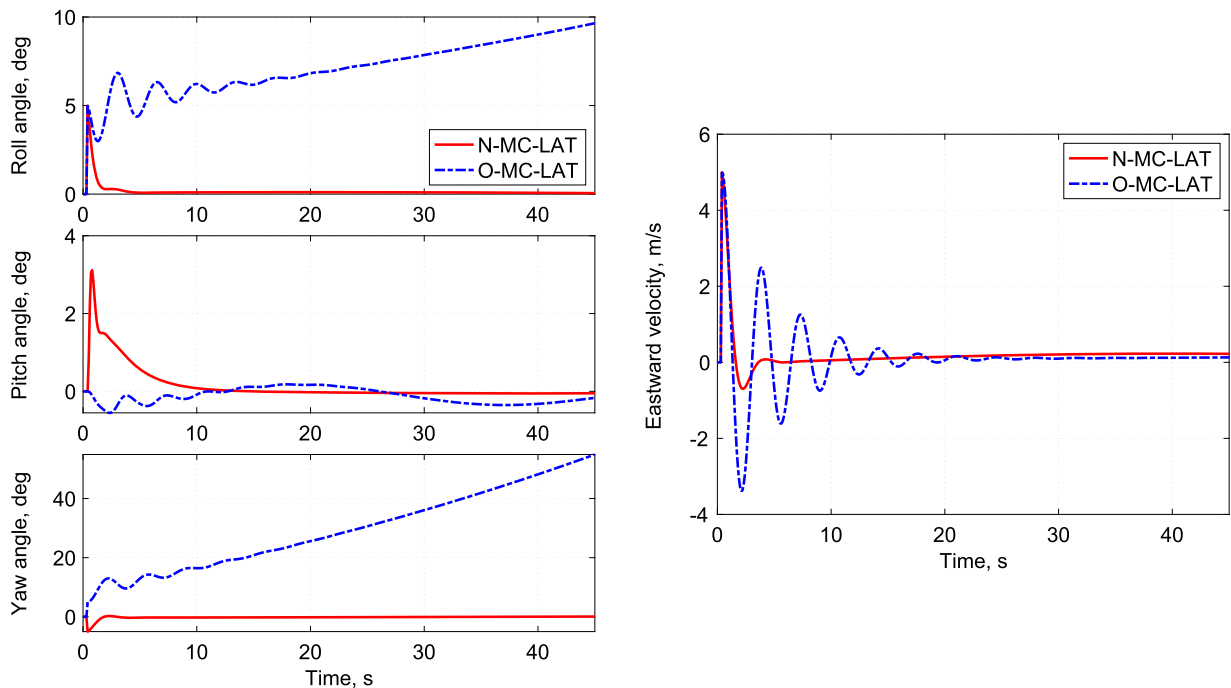


Fig. 7. Euler angle and eastward velocity response during flight subjected to lateral disturbance.

ates from the original path due to the transient and asymmetric inputs (see Figs. 13 and 14). This transition period is longer when the rotor acceleration is smaller; therefore, the conventional control surface inputs, mainly the rudder, are also used to adjust the flight path.

The Euler angles of the vehicle of all the simulated cases are presented in Fig. 13. The NMPC aims to track the vehicle's Euler angles, with the reference being the initial trimmed Euler angles. The case that performs better is the one with a higher spin acceleration (N-FR-S3000-F). Fig. 14 illustrates that, as the aircraft takes longer to reach the target rotor spin rate, it deviates more from the desired path, necessitating additional time and larger system inputs to bring the vehicle back to the reference flight path.

As can be derived, the best-case scenario would be an instantaneous spin rate change in the rotors with an infinite large spin acceleration. However, eVTOL rotors can't have an infinite spin acceleration with currently available technology. In addition, the range of achievable spin accelerations for eVTOL rotors is not well documented in the litera-

ture. While the maximum angular acceleration of a propeller can be determined by dividing the maximum torque by the propeller's moment of inertia, that information alone is not enough to determine a rotor's angular acceleration limit. Aircraft drag and propeller efficiency also greatly affect the determination of rotor spin acceleration limits. Detailed information on the performance and efficiency of eVTOL rotors is not publicly available as these aircraft are currently in the development phase [24–26]. Therefore, the spin acceleration of 1000 deg/s^2 is selected in the following studies as a more conservative choice that still presents acceptable path-tracking results with the NMPC. However, an even more conservative selection may be more realistic, which means degradation of controller success in following the desired flight path.

4.3. Tiltrotor tilt rate study

This study examines the impact of rotor tilt rate on the performance of the NMPC controller. Four tilt rates are evaluated, including 2, 5, 10,

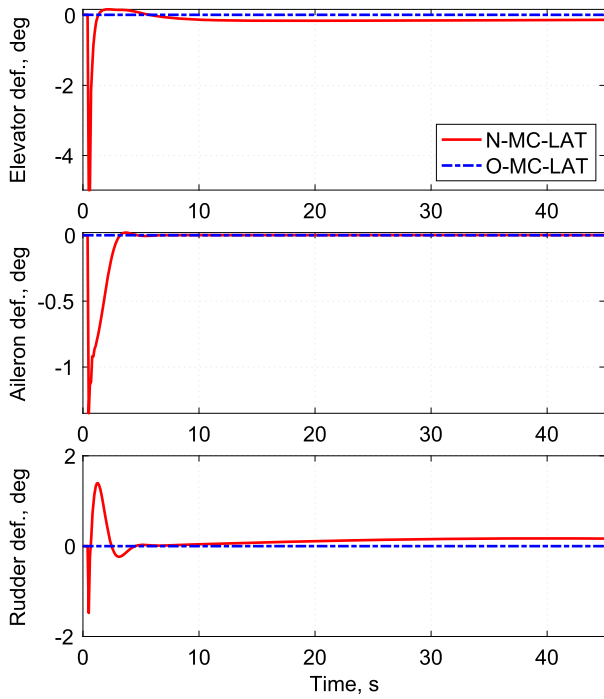


Fig. 8. Control surface inputs during flight subjected to lateral disturbance.

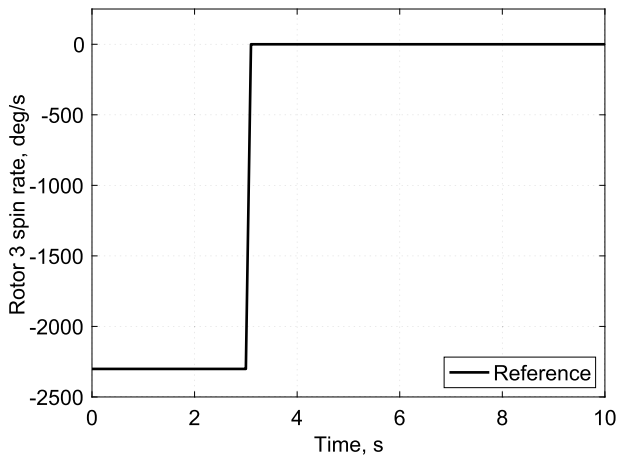


Fig. 9. Spin rate input for rotor 3 during asymmetric tiltrotor failure.

and 20 deg/s, with Case IDs listed in Table 6. The same initial flight condition and failure as Sec. 4.2 is used, except that rotors 5 and 6 initially face upward ($\Xi_{5;6} = 90^\circ$). This scenario requires rotors 5 and 6 to tilt forward to provide the trust for the vehicle. The rotor spin accelerations are set to the high value of 35,000 deg/s² for a nearly instantaneous spin rate shift. Therefore, the tilt rates of rotors 5 and 6 become the dominant impact factor on the aircraft's path-tracking performance. The input vector is extended to include rotor 5 and 6's tilt angles (Ξ_5 and Ξ_6), i.e.,

$$\mathbf{u}^T = \Delta \{ \delta_e \quad \delta_a \quad \delta_r \quad \Xi_5 \quad \Xi_6 \quad \dot{\Gamma}_3 \quad \dot{\Gamma}_4 \quad \dot{\Gamma}_5 \quad \dot{\Gamma}_6 \} \quad (24)$$

The open-loop response with rotors 5 and 6 initially upward is almost identical to the Case O-FR-F shown in Fig. 10. This is because the change in rotor orientation (facing upward instead of forward) only slightly alters the mass distribution on the aircraft.

Rotors 5 and 6 tilt from 90° (facing upward) to 0° (facing forward). Figs. 15 and 16 show this transition with different tilt rates, in addition to the near-instantaneous spin rate change. Elevator, aileron, and rudder

Table 6

Case ID and descriptions for rotor tilt rate study.

Case ID	Description
O-FR-U	Open loop
N-FR-T2-U	NMPC - tilt rate of 2 deg/s
N-FR-T5-U	NMPC - tilt rate of 5 deg/s
N-FR-T10-U	NMPC - tilt rate of 10 deg/s
N-FR-T20-U	NMPC - tilt rate of 20 deg/s

Table 7

Case ID and descriptions for asymmetric tiltrotor failure.

Case ID	Description
O-FR-F	Open loop - Rotors 5 and 6 initially angled forward
O-FR-U	Open loop - Rotors 5 and 6 initially angled upward
N-FR-F	NMPC - Rotors 5 and 6 initially angled forward
N-FR-U	NMPC - Rotors 5 and 6 initially angled upward

inputs are shown in Fig. 17. Note that the cases with lower tilt rates (2 and 5 deg/s) correspond to higher control surface input magnitudes.

Figs. 18 and 19 show the orientation and position of the aircraft with different tilt rates. The case that better tracks the Euler angle is the one with a larger tilt rate of 20 deg/s (N-FR-T20-U). This phenomenon is also observed in the aircraft's position tracking. On the other hand, the case with a low tilt rate may not be able to follow the desired path even with higher control surface inputs, as shown by Case N-FR-T2-U. In other words, even after rotors 5 and 6 have completed the tilt transition to the forward position, the aircraft is still not able to return to the straight flight path due North during the simulation time.

The case with a higher rotor input change rate once again yielded the best control results. However, such a high input rate may not be practical for real eVTOL aircraft. In literature, there is an eVTOL UAV platform [27] reported with a tilting rate of 14 deg/s. Nevertheless, a conservative value of 5 deg/s is selected in the following studies, as it has resulted in a reasonable trajectory tracking of the aircraft.

4.4. Asymmetric tiltrotor failure

With rotors spin acceleration of 1000 deg/s² and tilt rate of 5 deg/s, the aircraft is stabilized after a failure of rotor 3 occurs, while two different initial orientations of rotors 5 and 6 are considered, namely initially angled forward (Sec. 4.4.1) and initially upward (Sec. 4.4.2). The input vector of Eq. (24) is used, and the Case IDs and description are listed in Table 7.

4.4.1. Tiltrotor 3 failure with back rotors initially forward

Rotors 5 and 6 are activated following the failure of rotor 3. They operate as push thrusters immediately after the failure, and since they are initially oriented forward, no tilt adjustment is required.

In this scenario, the performance of the NMPC is compared with that of the linear MPC. As previously noted, the system states and outputs used for both controllers are defined in Eq. (21). The NMPC input vector is given by Eq. (24), while the MPC formulation omits $\dot{\Gamma}_3$, the variable associated with the failed rotor, from its input set. The diagonal values of the MPC weight matrices \mathbf{Q}_M and \mathbf{R}_M are listed in Table 8. Both controllers are simulated using a time step of 0.1 s and a prediction horizon of 10. For solving the underlying optimization problem, both NMPC and linear MPC employ MATLAB's *fmincon* solver, which is designed to minimize constrained nonlinear scalar functions.

The aircraft responses are shown in Figs. 20 and 21, where the cross symbol indicates the moment the aircraft crashes in the open-loop simulation. Additionally, the plus symbol marks the point at which the linear MPC solution becomes infeasible.

The results show that the NMPC can track the desired path with a minimal loss of altitude, in contrast to the open-loop response, where a

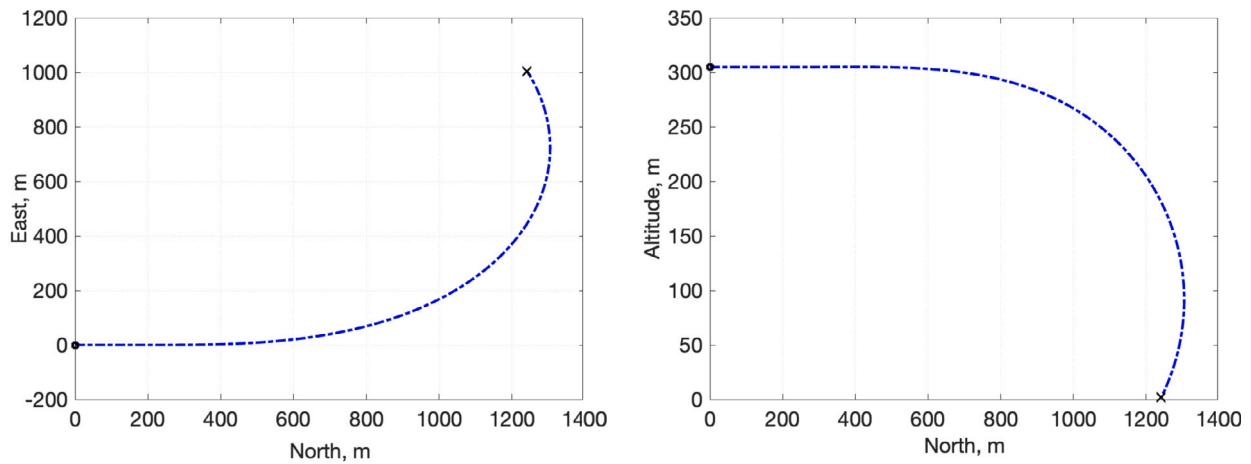


Fig. 10. Open-loop trajectory during asymmetric tiltrotor failure with tiltrotors 5 and 6 forward (O-FR-F).

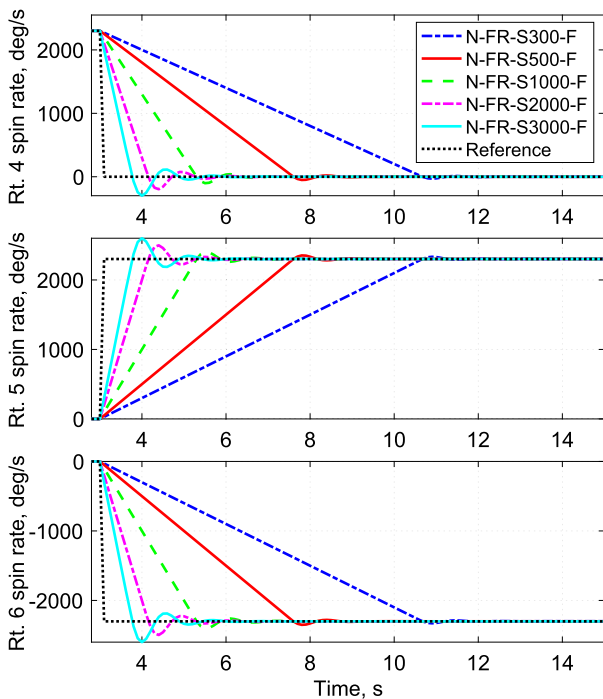


Fig. 11. Rotors spin rates during flight with asymmetric tiltrotor failure for different rotor spin accelerations.

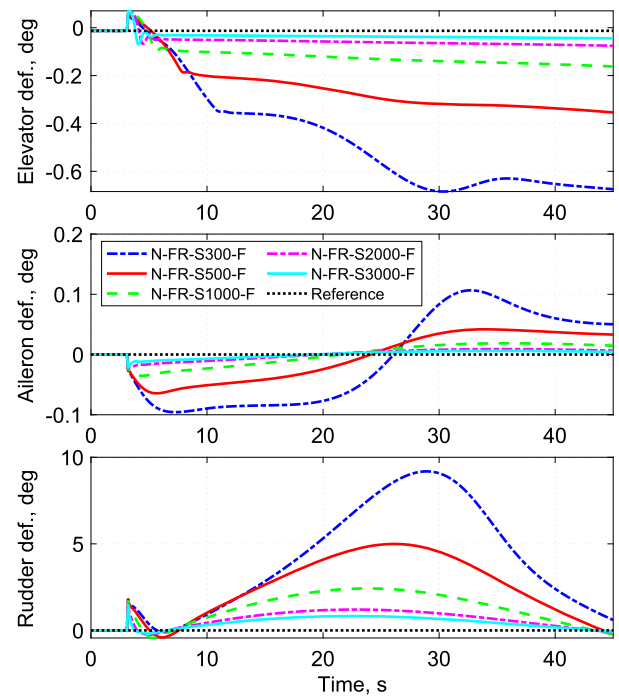


Fig. 12. Control surface inputs during flight with asymmetric tiltrotor failure for different rotor spin accelerations.

Table 8

Parameter of LQR and MPC for the vibration suppression simulation case.

Property	Value
Q_1, Q_3 to Q_6, Q_{10}, Q_{11}	1
Q_2	100
Q_7 to Q_9	10
R_1	10
R_2, R_3	1
R_4, R_5	100
R_6 to R_8	0.1

quick loss of altitude until a crash is observed. The NMPC also successfully maintains the Euler angles near constant, showing that even with a realistic rotor tilt rate and spin acceleration, the NMPC can track the path after a rotor failure. In comparison, while the linear MPC does mitigate the rapid altitude loss seen in the open-loop case, it performs less

effectively than the NMPC. Specifically, the MPC response exhibits an approximate 150 m altitude drop and initial oscillations in the roll and pitch angles.

Figs. 22 and 23 display the tiltrotor inputs for open-loop and controlled cases. The NMPC keeps the tilt angle of rotors 5 and 6 nearly constant in the forward position while adjusting their spin rate to the desired value as quickly as possible, considering the spin acceleration limit imposed on the controller. The linear MPC exhibits a similar behavior, although it shows a larger deviation in tilt angle as the simulation progresses. The control surface inputs are presented in Fig. 24. Throughout the simulation, NMPC commands mostly use the rudder for flight control, whereas linear MPC distributes control effort more evenly between the rudder and aileron. Notably, the elevator deflection does not reach a steady-state value in either controller, indicating that trimmed flight is not fully achieved and that the aircraft continues to adjust its pitch over time. Overall, the NMPC demonstrated a superior ability to maintain level flight following rudder failure compared to the MPC.

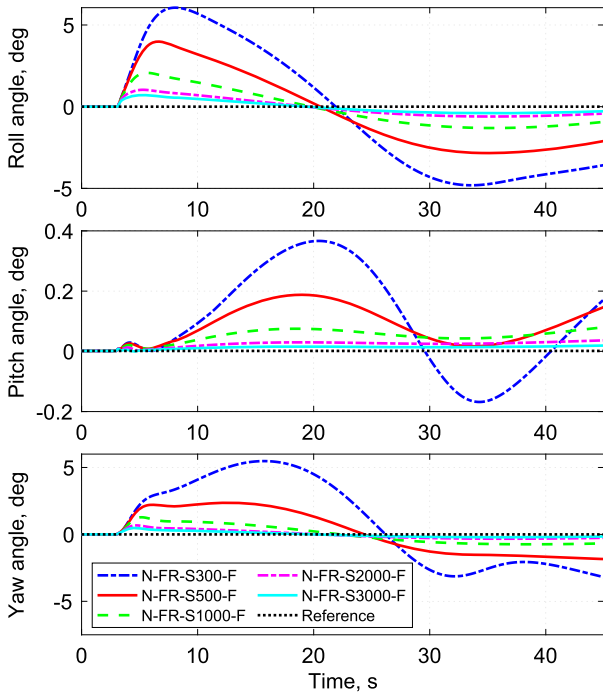


Fig. 13. Euler angle response during flight with asymmetric tiltrotor failure for different tiltrotor spin accelerations.

More importantly, identifying MPC settings that enabled full simulations without infeasibility proved to be challenging. Even adjusting the MPC weight matrices \mathbf{Q}_M and \mathbf{R}_M , varying the simulation time step, or altering the MPC prediction horizon did not lead to feasible solutions during the full simulation duration. This suggests that while a feasible operating region for the linear MPC under this level of system disturbance may exist, it is very narrow. Similar behavior was observed in the vibration suppression mission described in [19]. Consequently, the linear MPC formulation employed here is deemed unsuitable for applications involving higher excitation levels. Therefore, MPC will be omitted from the subsequent studies, which involve more challenging scenarios.

4.4.2. Tiltrotor 3 failure with back rotors initially upward

In this study, tiltrotors 5 and 6 start in an upward position right after the failure of rotor 3. They must tilt from 90° to 0° while spinning up. It makes this simulation more complicated than in Sec. 4.4.1. The aircraft response is presented in Figs. 25 and 26, with the cross indicating the instant an altitude of zero is obtained for the open-loop simulation. The aircraft crashes in approximately 30 s without control. Figs. 27 to 29 show the control input for the open-loop and controlled cases. The NMPC can effectively adjust the rotor tilt angles and spin rate to accurately and promptly meet the target values. However, during the simulation, the elevator deflection reaches higher magnitudes of approximately -4.5° , which does not reach a steady value at the end of the simulation.

The reason for the growing elevator angle can be better understood by observing the aircraft response (Figs. 25 and 26). Even after meeting the rotors' target inputs, the aircraft still tends to lose altitude. To reduce the altitude loss, the NMPC increases the elevator deflection, causing a slight increase in the aircraft's pitch angle. Although a level flight after the failure of rotor 3 is not fully achieved with the simulation, the aircraft still follows the intended path and a safe flight is possible with the assistance of NMPC.

4.5. Elevator failure

Giving continuation to the assessment of the controller's ability to stabilize flight, the effect of an elevator defect is investigated. The de-

fect involves setting the elevator deflection to zero after 3 s of trimmed level flight, which triggers the excitation of the rigid body phugoid mode of vibration. Tiltrotors 5 and 6 are then made available to the NMPC to maintain the level flight condition and suppress the rigid-body vibration, as the main control surface for pitch angle stabilization (elevator) is no longer functional. All rotors are subjected to the same rotor spin acceleration of 1000 deg/s^2 and tilt rate of 5 deg/s defined in Sec. 4.2 and 4.3.

Two cases are considered: one with the back rotors initially positioned upward (Sec. 4.5.1) and another with the back rotors initially positioned forward (Sec. 4.5.2). The Case ID and its descriptions are presented in Table 9 and the NMPC settings for these cases are outlined in the Appendix. Since this failure case induces a purely longitudinal motion, lateral motion, roll, and yaw angles are not presented herein.

4.5.1. Elevator failure with back rotors upward

The initial trimmed flight condition with rotors 5 and 6 in the upward position has a slightly positive elevator deflection, although it is close to zero. When the elevator fails and the deflection is instantly reduced to zero (see Fig. 30), the aircraft enters the phugoid mode of vibration. This is characterized by a low-frequency longitudinal rigid body vibration and a gradual loss of altitude. Additionally, the elevator is no longer available for pitch angle control, a task that must be taken over by rotors 5 and 6. To do this effectively, rotors 5 and 6 are maintained facing upward. Therefore, there is no need to tilt the rotors in this case, only requiring reaching the target spin rate. Figs. 31 and 32 show the inputs for the tiltrotors in both the NMPC and open-loop cases. The NMPC effectively adjusts the tiltrotors' spin rate to its target value while maintaining tilt angle in the upward position (90°). Tiltrotors 5 and 6 also exhibit a minor oscillation of tilt angle to reduce the rigid body vibration. This is achieved while adhering to the tilt rate and spin acceleration limitations mentioned previously. Overall, the controller demonstrates its capability to sustain the pitch angle and altitude at near-constant levels (see Fig. 33), showing minimal oscillation throughout the simulation.

In contrast, the response without control aid, in which the inputs are maintained at their initial values, displays noteworthy oscillations in pitch angle. These oscillations persist throughout the 180 s of simulation, with slow damping. Additionally, the open-loop altitude demonstrates significant oscillations and a continual decline, which is anticipated to continue beyond the simulation period.

Fig. 33 shows that the NMPC effectively decreases the pitch angle vibration in comparison to the open-loop response (O-FE-U). Although there is still some oscillation, the pitch angle range is minimal, of 0.007° compared to 0.18° for the open loop. The altitude is also being successfully maintained at a nearly constant level.

4.5.2. Elevator failure with back rotors forward

When the rear rotors are facing forward, the slight change in weight distribution in the aircraft causes the aircraft's trimmed flight condition to result in an initially negative elevator deflection. This deflection is instantaneously changed to zero when the elevator failure occurs (see Fig. 34). Although the initial elevator deflection is small, this change affects the phugoid mode vibration, causing an upward motion rather than downward (as discussed in Sec. 4.5.1). Since rotors 5 and 6 are initially oriented forward, they must tilt into the upward orientation to act effectively for pitch angle correction. Therefore, this case is more challenging than the one presented in the previous section, as the tilt transition time can lead to increased flight path deviation.

Two NMPC cases are being investigated. In Case N-FE-1-F, the target curves provided to the NMPC show changes in rotor spin rate and tilt angle starting at the instant of failure ($t = 3 \text{ s}$). In Case N-FE-2-F, the rotors begin to spin toward their target value after they have achieved their final tilt angle. In other words, rotors' tilt transition start at $t = 3 \text{ s}$ with no spin, while they start to spin at $t = 22 \text{ s}$.

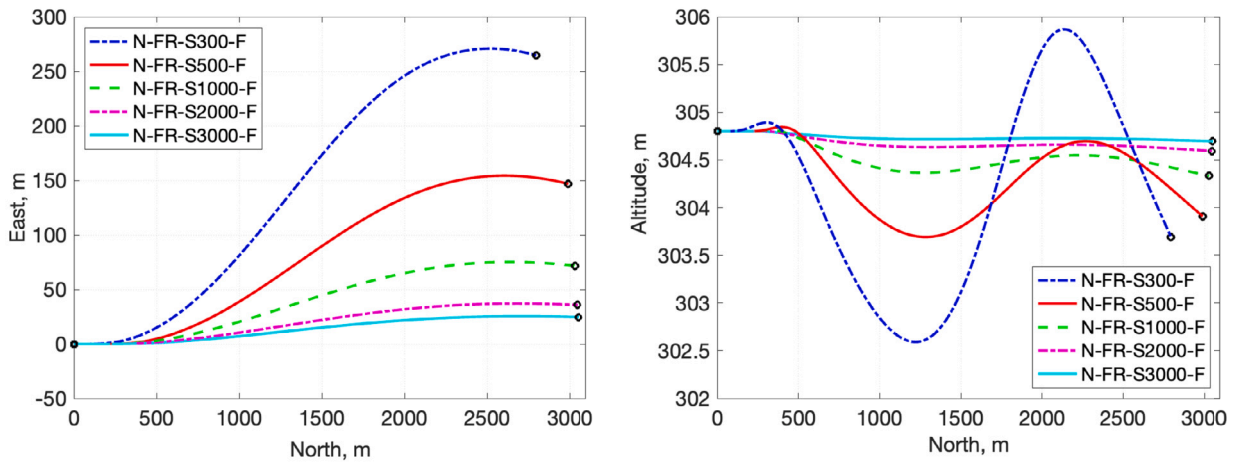


Fig. 14. Aircraft trajectory response during flight with asymmetric tiltrotor failure for different tiltrotor spin accelerations.

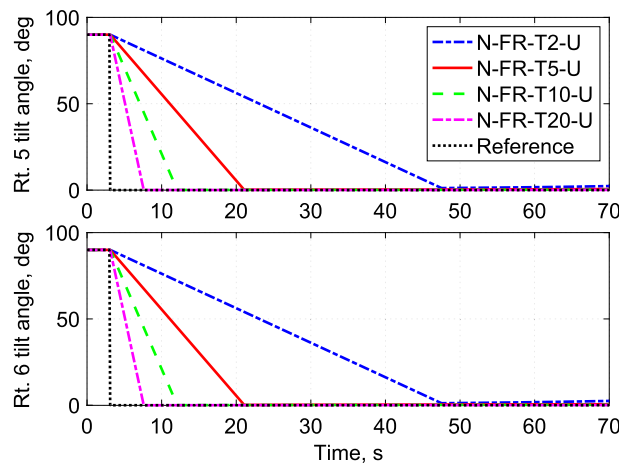


Fig. 15. Rotors tilt angle during flight with asymmetric tiltrotor failure for different tilt rates.

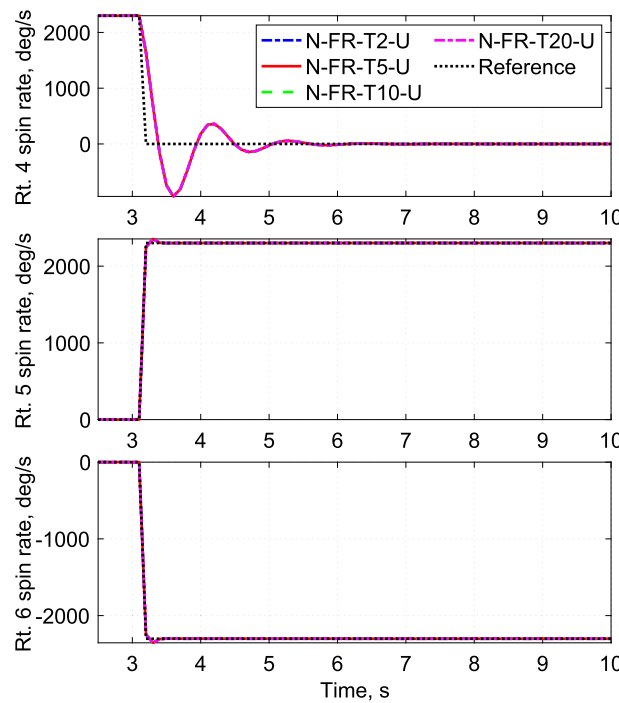


Fig. 16. Rotors spin rate during flight with asymmetric tiltrotor failure for different tilt rates.

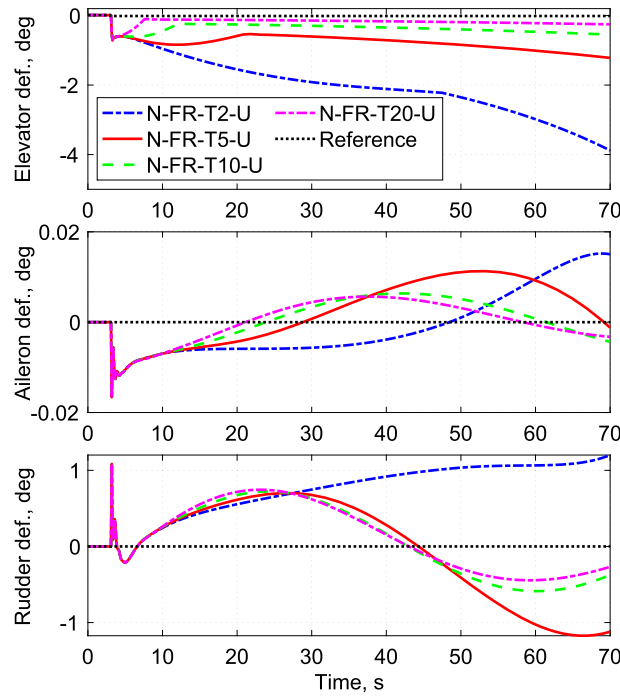


Fig. 17. Control surfaces inputs during flight with asymmetric tiltrotor failure for different tiling rates.

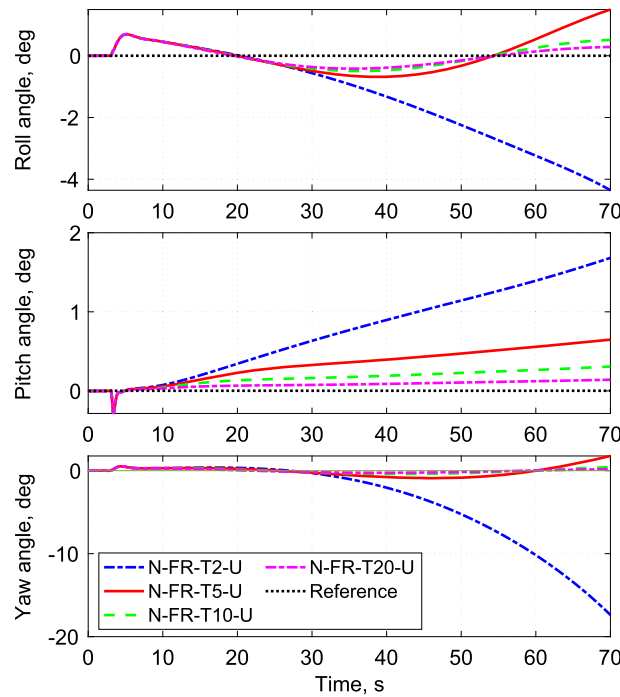


Fig. 18. Euler angle response during flight with asymmetric tiltrotor failure for different tilt rates.

Table 9
Case ID and descriptions for elevator failure.

Case ID	Description
O-FE-U	Open loop - Rotors 5 and 6 initially angled upward
O-FE-F	Open loop - Rotors 5 and 6 initially angled forward
N-FE-U	NMPC - Rotors 5 and 6 initially angled upward
N-FE-1-F	NMPC - Rotors 5 and 6 initially upward, spin and tilt simultaneously
N-FE-2-F	NMPC - Rotors 5 and 6 initially upward, spin after tilt

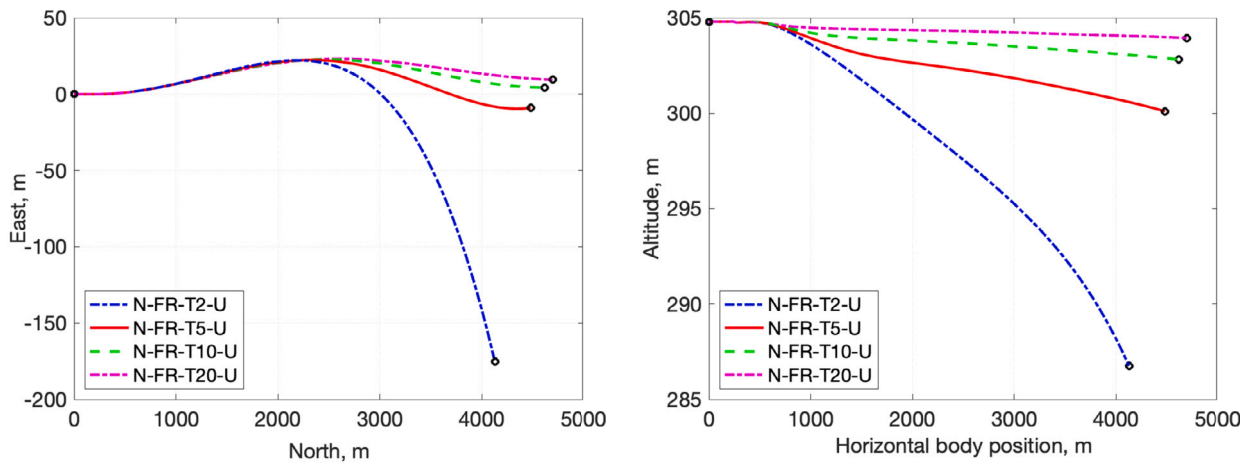


Fig. 19. Aircraft trajectory response during flight with asymmetric tiltrotor failure for different tilt rates.

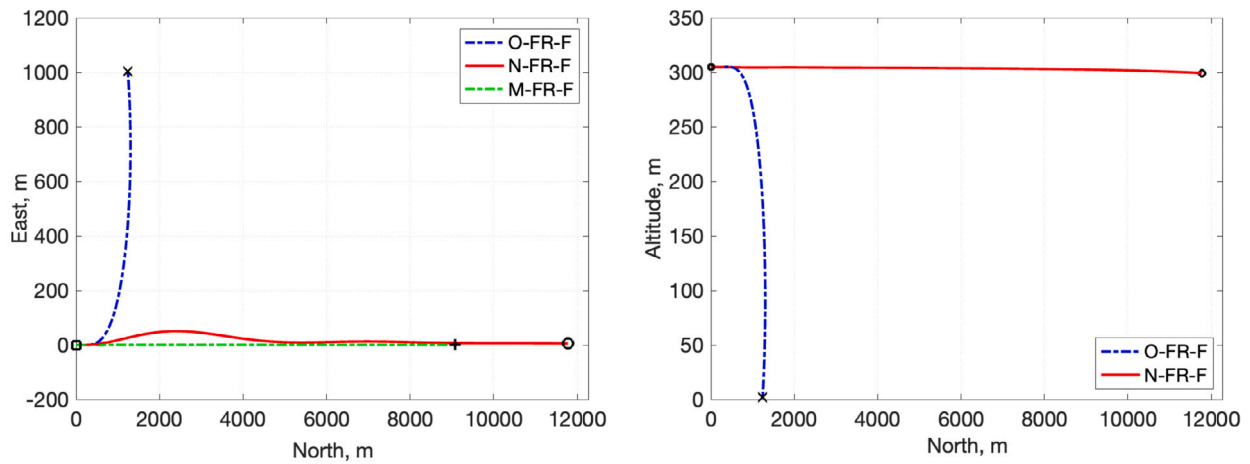


Fig. 20. Aircraft trajectory response during flight with asymmetric tiltrotor failure, back tiltrotors angled forward.

Fig. 34 shows that the tilt angle input is the same for both NMPC cases. In both cases, the target is reached and maintained for the rest of the simulation. Fig. 35 shows the rotors' spin rates. In case N-FE-1-F, rotors 5 and 6 are turned on at 3 s into the simulation, while in case N-FE-2-F, they are activated at 22 s. Note that both NMPC cases use the spin rate of rotors 3 and 4 to eliminate rigid body vibration, with the N-FE-2-F case reaching higher magnitudes after the start of the transition.

Figs. 35 and 36 show the rotor inputs for both controller cases and the case without controller (constant inputs). In addition to the tilt angle and spin rate transition into target value, the controller also uses a small oscillation of rotors 3 and 4 spin rate for vibration suppression.

The system responses for N-FE-1-F (Fig. 37) show that when rotors 5 and 6 start to spin and tilt into their respective target values simultaneously, the aircraft exhibits a higher magnitude of pitch angle oscillation compared to the open-loop response. Consequently, a higher altitude oscillation is also observed. In addition, the altitude also oscillated around an altitude of approximately 306 m, which is higher than the desired 304.8 m. This deviation, along with the rigid body oscillation, is not successfully suppressed by the NMPC during simulation. In contrast, Case N-FE-2-F, which involves the rotors' spinning after tilting into the orientation, exhibits a good path-tracking response. Although this case does not completely eliminate rigid body vibration during the simulation, it does demonstrate faster vibration suppression. There is a decrease in pitch angle magnitude of 1.1×10^{-3} deg/s compared to the natural damping of the pitch angle of 2.2×10^{-4} deg/s for the open-loop re-

sponse and 7.8×10^{-4} deg/s for the N-FE-1-F case. This suggests that isolating the inputs for the NMPC can be beneficial in certain scenarios, highlighting the importance of an in-the-loop path generator capable of determining the best combination of inputs for the NMPC to track. The results also imply that relying solely on four tiltrotors to compensate for the loss of the elevator may not be adequate in more demanding situations, such as when the rotors need to tilt to the required angle before spinning. The inclusion of the front tiltrotors (refer to 1 and 2 of Fig. 3) may aid in pitch correction, potentially reducing the time required to eliminate the phugoid mode vibration.

4.6. Computational cost

While the results presented here demonstrate the effectiveness of NMPC for eVTOL control, the high computational cost remains a significant challenge, limiting its real-time applicability during flight. Currently, simulating a 60 s flight requires approximately 10 h of computation time. This involves a system with 13 states, nine inputs, and five outputs, simulated with a 0.1 s time step, a prediction horizon of 10, and a control horizon of 1, conditions consistent with those in Sec. 4.2 onward. The average computation time per time step is 68.25 s, with 99% of that dedicated to NMPC calculations (67.6 s), and only 1% spent on plant simulation and data storage for the subsequent step. By contrast, the MPC averages 1.6 s per time step, with 64.6% of that time (1.07 s) devoted to controller calculations.

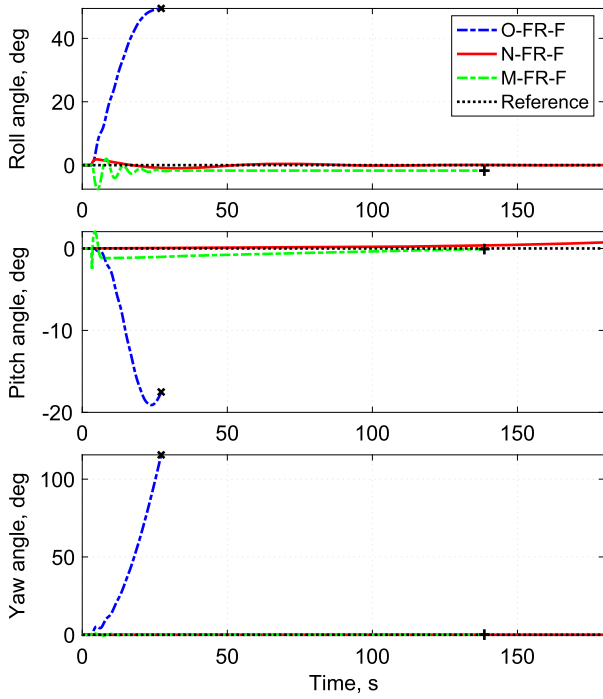


Fig. 21. Euler angle response during flight with asymmetric tiltrotor failure, back tiltrotors angled forward.

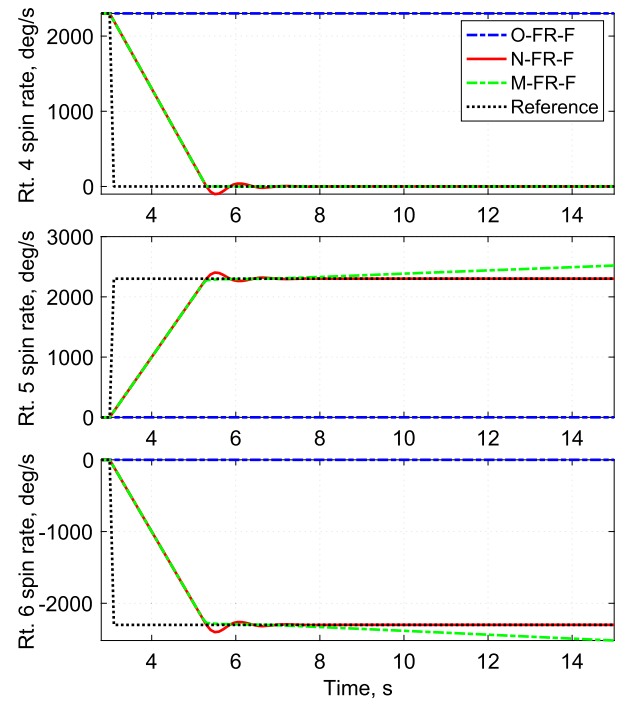


Fig. 23. Rotors spin rate during flight with asymmetric tiltrotor failure, back tiltrotors angled forward.

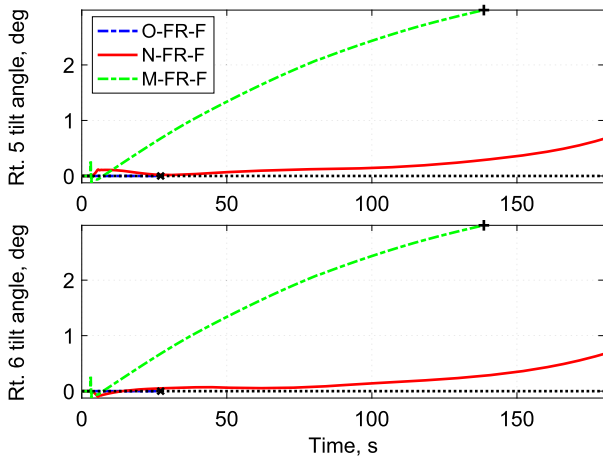


Fig. 22. Rotors tilt angle during flight with asymmetric tiltrotor failure, back tiltrotors angled forward.

This stark difference highlights the primary limitation of NMPC and underscores the need for further research into computational optimization. As previously noted, factors such as the prediction horizon, control horizon, simulation time step, and input constraints significantly influence NMPC's computational burden. Therefore, a comprehensive parametric study examining these elements is essential for controller optimization.

Although the efficient computation of NMPC is not the focus of this work, it is worth discussing the recent works that could be used to further improve this work. One approach is to accelerate the computations by relaxing inequality constraints [28], deriving shortest prediction horizon with stability guarantee [29,30]. Another approach is to replace the nonlinear dynamic model with other model representations that will lead to efficient computations, including LPV model [13], Artificial neural networks (ANN) [31], and Koopman operator model [32]. Besides, deep learning provides an alternative way to infer an approximate model and self-tune the controller [33]. These approaches are of

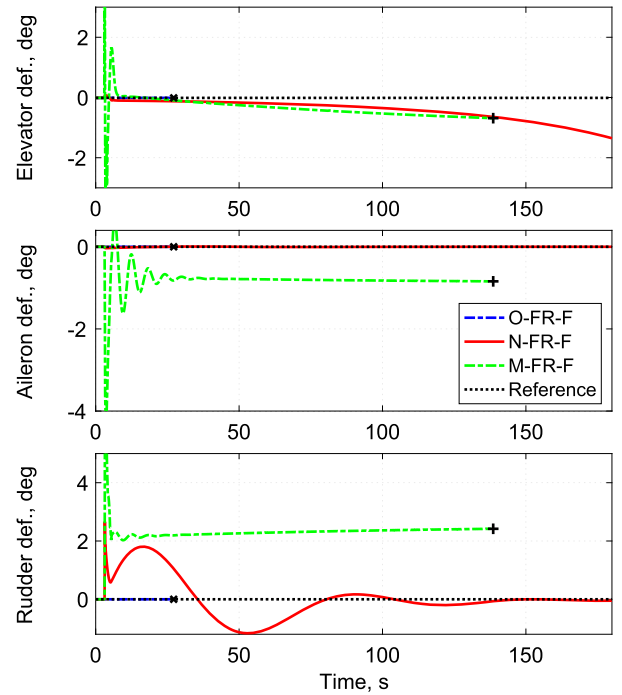


Fig. 24. Control surfaces inputs during flight with asymmetric tiltrotor failure, back tiltrotors angled forward.

special interest for eVTOL applications in real-time implementation of MPC algorithms, but need special attention on stability and robustness for flight safety.

5. Conclusion

In this paper, the implementation of a Nonlinear Model Predictive Controller (NMPC) for an urban air mobility aircraft during level flight with control input failure is presented. The study first focused on the

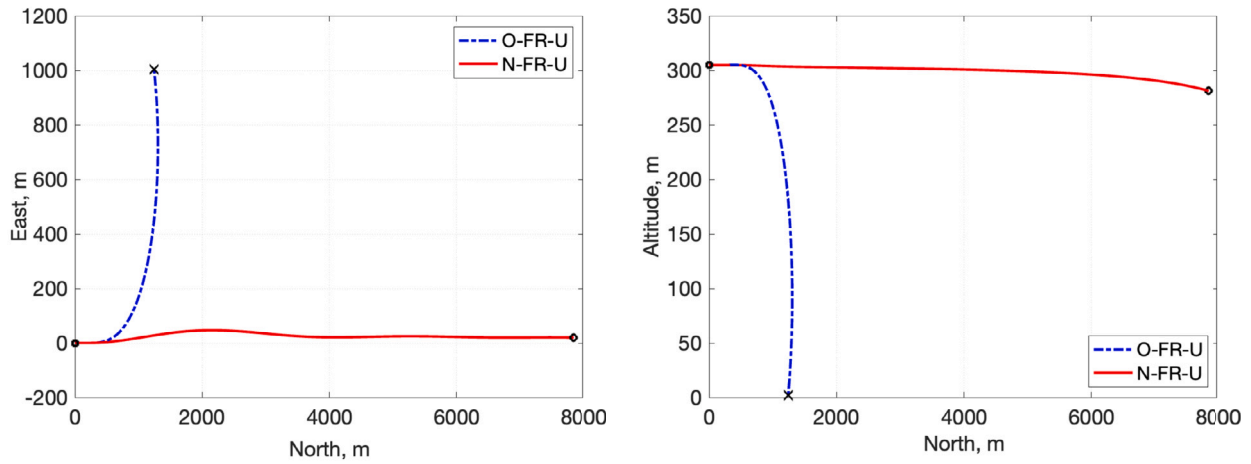


Fig. 25. Aircraft trajectory response during flight with asymmetric tiltrotor failure, back tiltrotors angled upward.

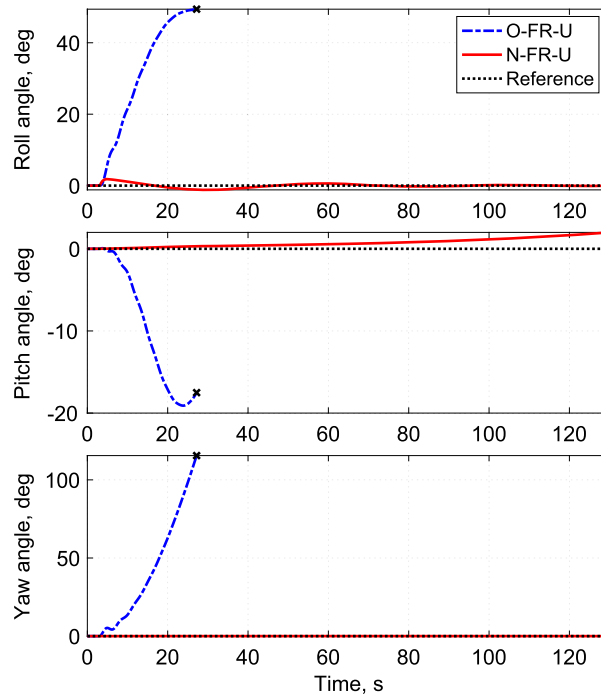


Fig. 26. Euler angle response during flight with asymmetric tiltrotor failure, back tiltrotors angled upward.

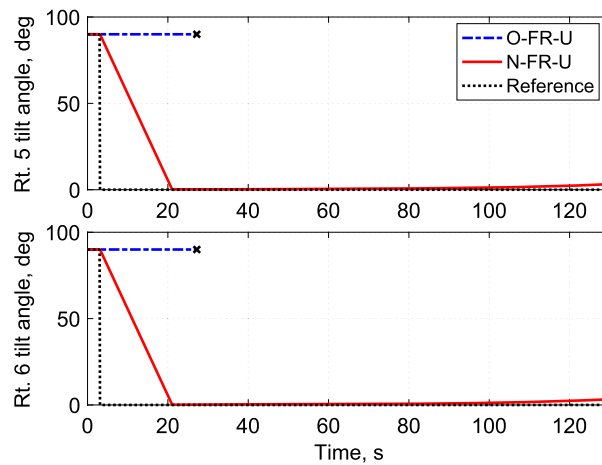


Fig. 27. Rotors tilt angle during flight with asymmetric tiltrotor failure, back tiltrotors angled upward.

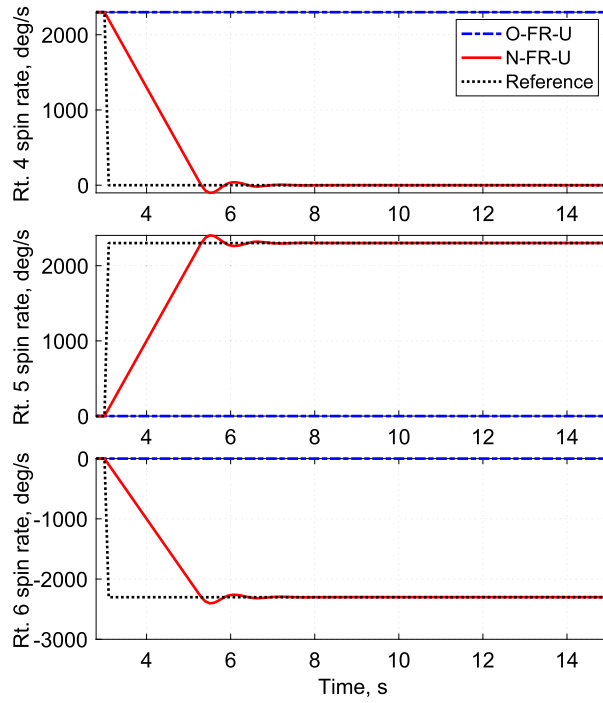


Fig. 28. Rotors spin rate during flight with asymmetric tiltrotor failure, back tiltrotors angled upward.

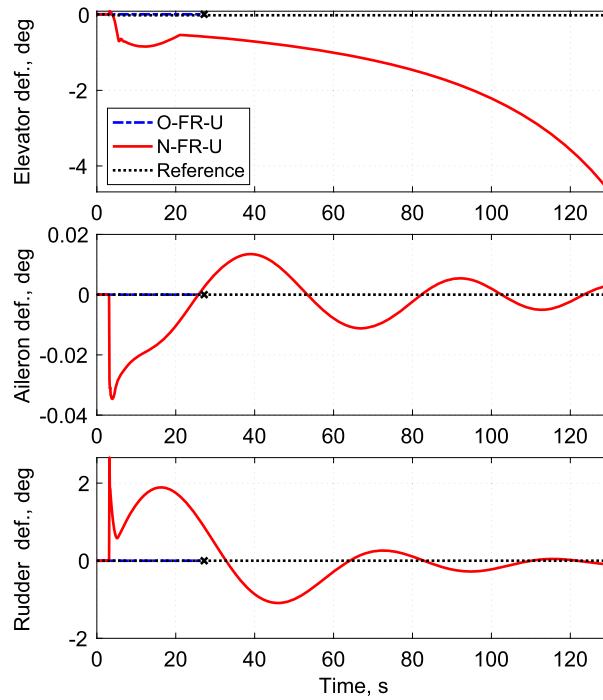


Fig. 29. Control surfaces inputs during flight with asymmetric tiltrotor failure, back tiltrotors angled upward.

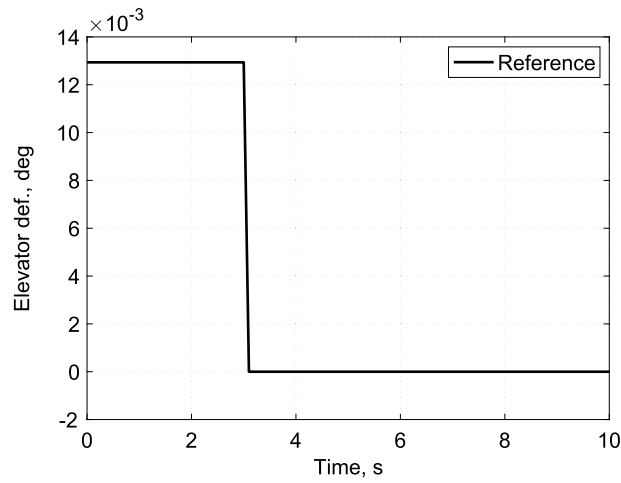


Fig. 30. Elevator deflection input with failure, back tiltrotors forward.

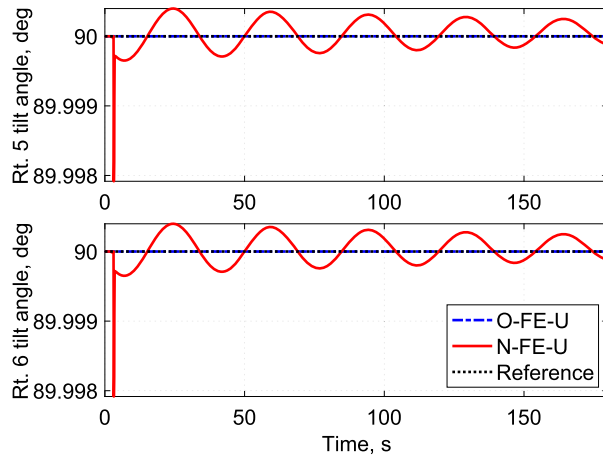


Fig. 31. Tiltrotor 5 and 6 tilt angle input during flight with elevator failure, back tiltrotors upward.

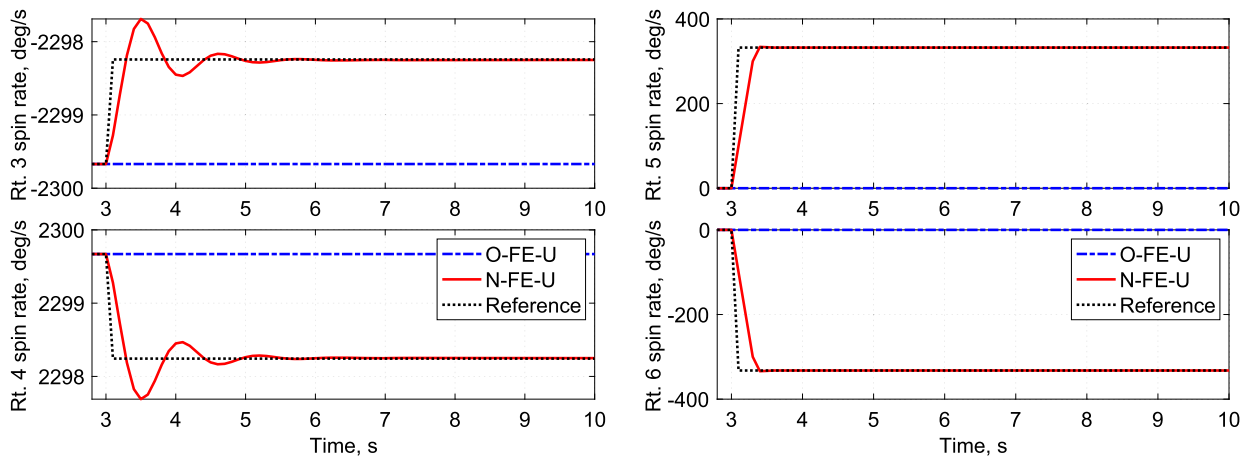


Fig. 32. Tiltrotor spin rate during flight with elevator failure. Back tiltrotors positioned upward.

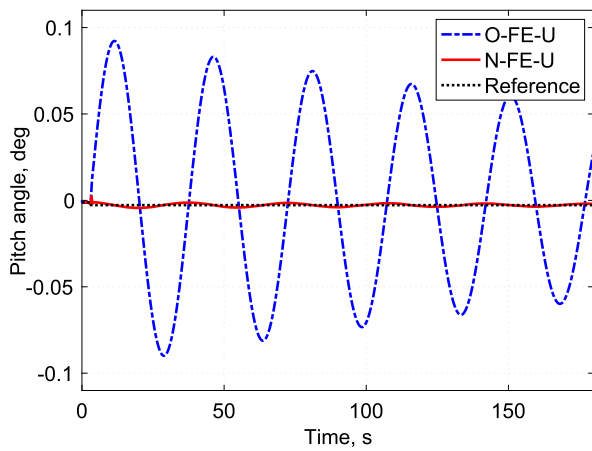


Fig. 33. System response during flight with elevator failure. Back tiltrotors positioned upward.

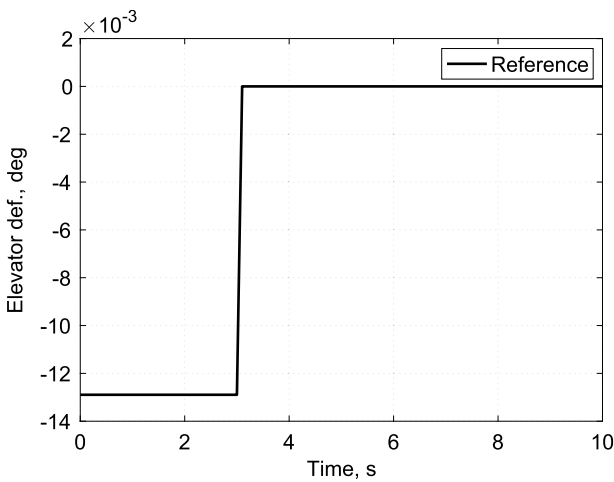
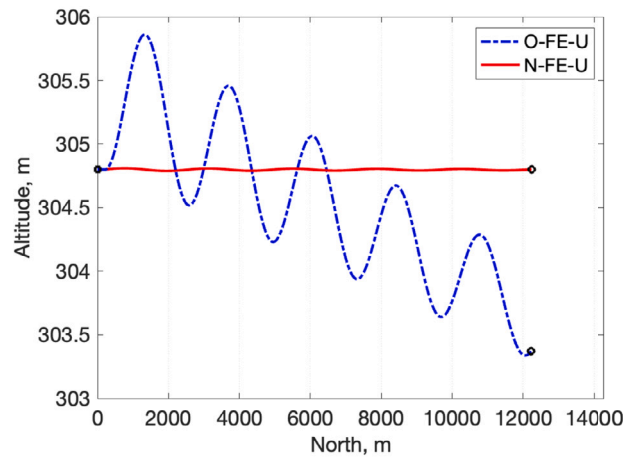


Fig. 34. Elevator deflection input with failure, back tiltrotors forward.

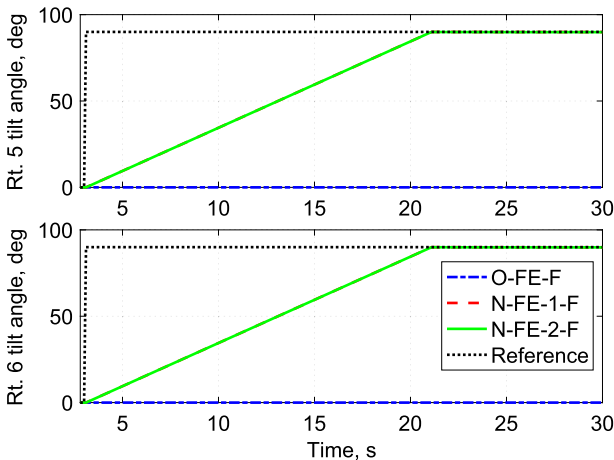


Fig. 35. Tiltrotor 5 and 6 tilt angle input during flight with elevator failure. Back tiltrotors positioned forward.

study of the NMPC stability and performance through the Monte Carlo method, where each system output was subjected to variations and the controller was tasked with returning such outputs to the initial trimmed flight condition. The results show that the controller is stable and able to converge to the desired values for most outputs, with a fast response

time of less than 7 ms, only not being able to fully converge for the longitudinal velocity, yaw angular velocity, and lateral aircraft position. The case for the longitudinal velocity converged to a value slightly different from the target; the case for yaw angular velocity converged to a solution but only to variations of $\pm 2^\circ$; the case for lateral velocity did not fully converge during 30 s simulation. However, none of the solutions diverged. Two scenarios involving simultaneous variation of multiple outputs were presented, one with longitudinal disturbances and another with lateral disturbances. For both cases, the controller did not diverge and was able to return the flight to an approximately trimmed condition, even under such challenging conditions.

The impact of rotor spin acceleration and tilt rate on flight control was also investigated. It was found that a faster input rate of change is beneficial for the NMPC. However, both the spin acceleration and tilt rate are limited by motor capabilities, aircraft, and propeller design. Therefore, the more conservative settings of 1000 deg/s^2 spin acceleration and 5 deg/s tilt rate were selected for the following simulations, which still showed good path-tracking results when analyzed with asymmetric rotor failure.

Two failure cases were analyzed with the aforementioned rotor settings: asymmetric tiltrotor and elevator failures during level flight. Both were simulated with the back rotors initially oriented either upward or forward. In the rotor failure scenario, the back rotors function as push thrusters, making more challenging for the configuration with back rotors initially upward-facing due to the additional requirement of tilting into position while simultaneously reaching the target spin rate. The NMPC was compared with a linear MPC for the less challenging configuration, where the rotors were already facing forward. Results showed that the MPC was less effective than the NMPC in returning the aircraft to trimmed flight. The feasible operating region for the MPC under this level of system disturbance proved to be very narrow, making it unsuitable for applications involving high levels of excitation. In contrast, the NMPC successfully tracked the reference trajectories and maintained level flight in both initial rotor orientations following the failure, highlighting its robustness and superior performance under failure conditions.

Next, the elevator failure was analyzed considering the two positions of the back rotors. In this case, the back rotors act on pitch correction to remove the phugoid mode vibration excited by the elevator failure. The most challenging case was when the back rotors were initially forward, requiring tilting into position. The results showed that activating the back rotor before completing the tilting causes a more significant deviation from the desired flight path. Conversely, starting rotor spinning after tilting into position showed excellent results, which could be improved in the future by adding front rotors to assist further with pitch correction.

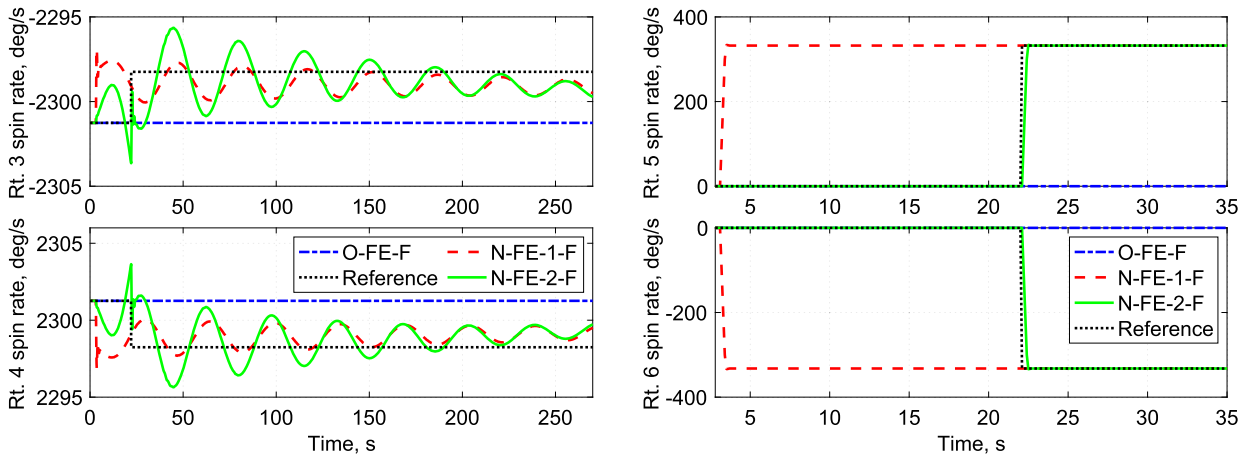


Fig. 36. Tiltrotor spin rate during flight with elevator failure. Back tiltrotors positioned forward.

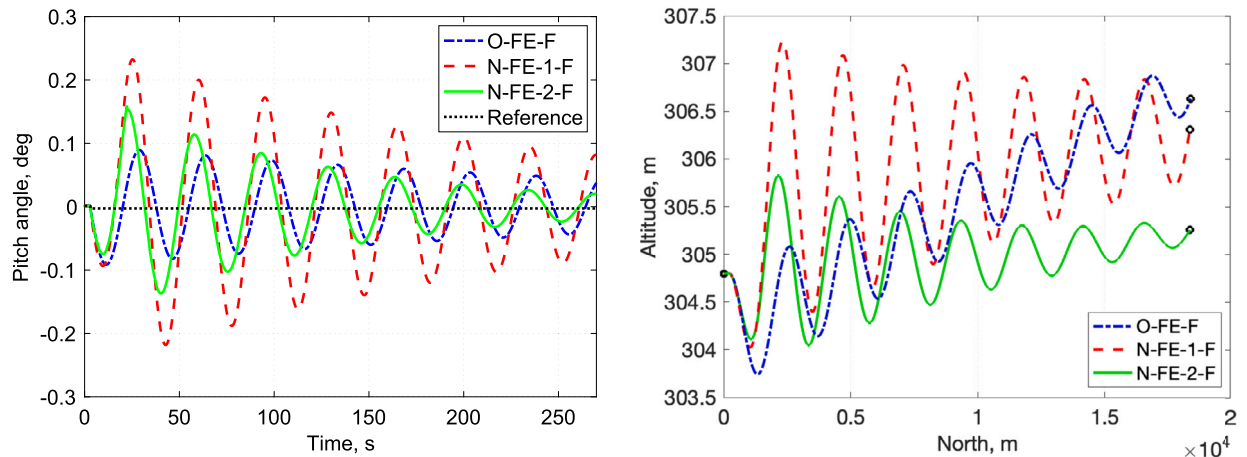


Fig. 37. System response during flight with elevator failure. Back tiltrotors positioned forward.

The high computation cost of NMPC remains a significant challenge of the proposed method. Currently, a 60 s flight simulation takes 10 h of computation time, preventing its application for real-time flight control. The use of Neural Network-based NMPC can reduce the time needed to achieve the NMPC optimal input solution by using a neural network approximation of the aircraft model for the NMPC future prediction, rather than the full system model. This approach is currently under investigation for future studies.

CRedit authorship contribution statement

Jessica S.M. Nunes: Writing – review & editing, Writing – original draft, Visualization, Methodology, Investigation, Formal analysis. **Wei-hua Su:** Writing – review & editing, Supervision, Project administration, Methodology, Investigation, Formal analysis. **Tianyi He:** Writing – review & editing, Supervision, Methodology, Formal analysis.

Declaration of competing interest

The authors declare that they have no known competing financial interests or personal relationships that could have appeared to influence the work reported in this paper.

Appendix A

The table below presents the summary of the NMPC settings for each simulation case presented herein.

- Case ID - 1-F2-3-3-4
 - 1: open-loop (O) or NMPC (N) simulations
 - 2: failure type. E for elevator and R for tiltrotor failure
 - 3: additional information
 - 4: initial position of the back tiltrotors. F for forward and U for upward
- Description
- Tiltrotor initial angle - 90° for upward
- t_f - length of simulation in seconds
- dt - simulation time step in seconds
- Input vector - applicable for NMPC. Open-loop uses all system inputs
- p - NMPC prediction horizon
- n - NMPC control horizon
- Output weight ω^y - weights for each y variable before and after control failure
- Output weight ω^u - weights for each u variable before and after control failure
- $\pm u_{lim}$ - upper and lower limits for NMPC inputs
- $\pm \Delta u_{lim}$ - upper and lower limits for NMPC input rate

Data availability

Data will be made available on request.

References

- [1] R. Goyal, C. Reiche, C. Fernando, J. Serrao, S. Kimmel, A. Cohen, S. Shaheen, Urban air mobility (UAM) market study, Tech. Rep. HQ-E-DAA-TN65181, National Aeronautics and Space Administration, 2018.
- [2] Y. Zhou, H. Zhao, Y. Liu, An evaluative review of the VTOL technologies for unmanned and manned aerial vehicles, *Comput. Commun.* 149 (2020) 356–369, <https://doi.org/10.1016/j.comcom.2019.10.016>.
- [3] A. Straubinger, R. Rothfeld, M. Shamiyeh, K.-D. Büchter, J. Kaiser, K.O. Plötner, An overview of current research and developments in urban air mobility – setting the scene for UAM introduction, *J. Air Transp. Manag.* 87 (2020) 101852, <https://doi.org/10.1016/j.jairtraman.2020.101852>.
- [4] Y. Zou, K. Xia, Robust fault-tolerant control for underactuated takeoff and landing UAVs, *IEEE Trans. Aerosp. Electron. Syst.* 56 (5) (2020) 3545–3555, <https://doi.org/10.1109/TAES.2020.2975446>.
- [5] C. Ke, K.-Y. Cai, Q. Quan, Uniform fault-tolerant control of a quadcopter with rotor failure, *IEEE/ASME Trans. Mechatron.* 28 (1) (2023) 507–517, <https://doi.org/10.1109/TMECH.2022.3202804>.
- [6] J. Mabboux, V. Pommier-Budinger, S. Delbecq, J. Bordeneuve-Guibé, Co-design of a multirotor UAV with robust control considering handling qualities and motor failure, *Aerosp. Sci. Technol.* 144 (2024) 108778, <https://doi.org/10.1016/j.ast.2023.108778>.
- [7] B. Wang, D. Zhu, L. Han, H. Gao, Z. Gao, Y. Zhang, Adaptive fault-tolerant control of a hybrid canard rotor/wing UAV under transition flight subject to actuator faults and model uncertainties, *IEEE Trans. Aerosp. Electron. Syst.* 59 (4) (2023) 4559–4574, <https://doi.org/10.1109/TAES.2023.3243580>.
- [8] J. Betancourt, V. Balaguer, P. Castillo, P. García, R. Lozano, Robust control scheme based on an uncertainty and disturbance estimator for a quadrotor with motor failures, *J. Field Robot.* 40 (5) (2023) 1115–1129, <https://doi.org/10.1002/rob.22174>.
- [9] C. Ke, K.-Y. Cai, Q. Quan, Uniform passive fault-tolerant control of a quadcopter with one, two, or three rotor failure, *IEEE Trans. Robot.* 39 (6) (2023) 4297–4311, <https://doi.org/10.1109/TRO.2023.3297048>.
- [10] M. Saied, H. Shraim, C. Francis, A review on recent development of multirotor UAV fault-tolerant control systems, *IEEE Aerosp. Electron. Syst. Mag.* 39 (9) (2024) 146–180, <https://doi.org/10.1109/MAES.2023.3327697>.
- [11] E.F. Camacho, C. Bordons, *Model Predictive Control*, 2nd edition, *Advanced Textbooks in Control and Signal Processing*, Springer, London, 2007.
- [12] B. Kouvaritakis, M. Cannon, *Model Predictive Control: Classical, Robust and Stochastic*, *Advanced Textbooks in Control and Signal Processing*, Springer, Cham, 2016.
- [13] S. Burton, T. He, W. Su, Trajectory planning and LPV model predictive control of tilt-rotor VTOL aircraft, in: 2023 American Control Conference (ACC), IEEE, 2023, pp. 2836–2841.
- [14] F. Nan, S. Sun, P. Foehn, D. Scaramuzza, Nonlinear MPC for quadrotor fault-tolerant control, *IEEE Robot. Autom. Lett.* 7 (2) (2022) 5047–5054, <https://doi.org/10.1109/LRA.2022.3154033>, publisher = IEEE.
- [15] S. Gros, R. Quirynen, M. Diehl, Aircraft control based on fast non-linear MPC & multiple-shooting, in: 51st IEEE Conference on Decision and Control (CDC), IEEE, 2012, pp. 1142–1147.
- [16] G. Zogopoulos-Papaliakos, G.C. Karras, K.J. Kyriakopoulos, A fault-tolerant control scheme for fixed-wing UAVs with flight envelope awareness, *J. Intell. Robot. Syst.* 102 (2) (2021) 46, <https://doi.org/10.1007/s10846-021-01393-3>.
- [17] A. Eltrably, D. Ichalal, S. Mammari, Quadcopter trajectory tracking in the presence of 4 faulty actuators: a nonlinear MHE and MPC approach, *IEEE Control Syst. Lett.* 6 (2021) 2024–2029, <https://doi.org/10.1109/LCSYS.2021.3137099>.
- [18] X. Chen, S. Wang, H. Zhao, K.-Y. Cai, Q. Quan, Fault-tolerant control of lifting-wing multicopter based on nonlinear MPC, *IEEE Robot. Autom. Lett.* (2025), <https://doi.org/10.1109/LRA.2025.3565364>.
- [19] J.S.M. Nunes, W. Su, T. He, Vibration suppression and trajectory tracking with nonlinear model predictive control for UAM aircraft, *J. Dyn. Syst. Meas. Control* 147 (4) (2025) 041010, <https://doi.org/10.1115/1.4067770>.
- [20] S. Qu, G. Zhu, W. Su, S.S.-M. Swei, M. Hashimoto, T. Zeng, Adaptive model predictive control of a six-rotor electric vertical take-off and landing urban air mobility aircraft subject to motor failure during hovering, *Proc. Inst. Mech. Eng., G J. Aerosp. Eng.* 236 (7) (2022) 1396–1407, <https://doi.org/10.1177/09544100211032434>.
- [21] W. Su, S. Qu, G. Zhu, S.S.-M. Swei, M. Hashimoto, T. Zeng, Modeling and control of a class of urban air mobility tiltrotor aircraft, *Aerosp. Sci. Technol.* 124 (2022) 107561, <https://doi.org/10.1016/j.ast.2022.107561>.
- [22] G. Takács, B. Rohal-Ilkiv, *Model Predictive Vibration Control: Efficient Constrained MPC Vibration Control for Lightly Damped Mechanical Structures*, Springer Science and Business Media, 2012.
- [23] E.F. Camacho, C. Bordons, *Model Predictive Control: Classical, Robust and Stochastic*, Springer International Publishing, 2016.
- [24] C. Reiche, C. McGillen, J. Siegel, F. Brody, Are we ready to weather urban air mobility UAM?, in: 2019 Integrated Communications, Navigation and Surveillance Conference (ICNS), IEEE, 2019, pp. 2E21–2E27.
- [25] S. Siewert, K. Sampigethaya, J. Buchholz, S. Rizzor, Fail-safe, fail-secure experiments for small UAS and UAM traffic in urban airspace, in: 2019 IEEE/AIAA 38th Digital Avionics Systems Conference (DASC), IEEE, 2019.
- [26] E. Xu, *The future of transportation: White paper on urban air mobility systems*, Tech. Rep., EHang, 2020.
- [27] C. Spencer, T. He, LPV system identification of VTOL aircraft with hybrid configuration, in: Proceedings of the ASME 2025 Aerospace Structures, Structural Dynamics, and Materials Conference, ASME, 2025.
- [28] D. Wang, Q. Pan, Y. Shi, J. Hu, C. Zhao, Efficient nonlinear model predictive control for quadrotor trajectory tracking: algorithms and experiment, *IEEE Trans. Cybern.* 51 (10) (2021) 5057–5068, <https://doi.org/10.1109/TCYB.2020.3043361>.
- [29] M.A. Goma, O. De Silva, G.K. Mann, R.G. Gosine, Computationally efficient stability-based nonlinear model predictive control design for quadrotor aerial vehicles, *IEEE Trans. Control Syst. Technol.* 31 (2) (2022) 615–630, <https://doi.org/10.1109/TCST.2022.3188399>.
- [30] M.A. Goma, O. De Silva, A. Jayasiri, G.K. Mann, Towards computationally efficient nmpc design with stability guarantee for learning-based dynamic models: a case study of UAVs, in: 2024 American Control Conference (ACC), IEEE, 2024, pp. 2122–2127.
- [31] J.H. Hoekstra, B. Cseppento, G.I. Beintema, M. Schoukens, Z. Kollár, R. Tóth, Computationally efficient predictive control based on ANN state-space models, in: 2023 62nd IEEE Conference on Decision and Control (CDC), IEEE, 2023, pp. 6336–6341.
- [32] M. Wang, X. Lou, W. Wu, B. Cui, Koopman-based MPC with learned dynamics: hierarchical neural network approach, *IEEE Trans. Neural Netw. Learn. Syst.* 35 (3) (2022) 3630–3639, <https://doi.org/10.1109/TNNLS.2022.3194958>.
- [33] T. Baumeister, S.L. Brunton, J. Nathan Kutz, Deep learning and model predictive control for self-tuning mode-locked lasers, *J. Opt. Soc. Am.* 35 (3) (2018) 617–626, <https://doi.org/10.1364/JOSAB.35.000617>.